PNNL-14779

Pacific Northwest
National Laboratory
Operated by Battelle for the
U.S. Department of Energy

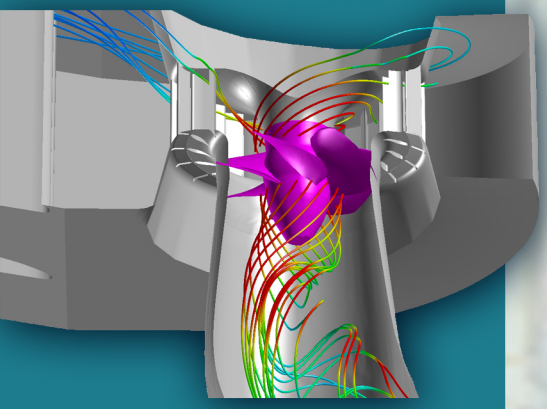

Six-Degree-of-Freedom Sensor Fish Design – Governing Equations and Motion Modeling

Z. Deng
M.C. Richmond
C.S. Simmons
T.J. Carlson
Pacific Northwest National Laboratory

July 2004

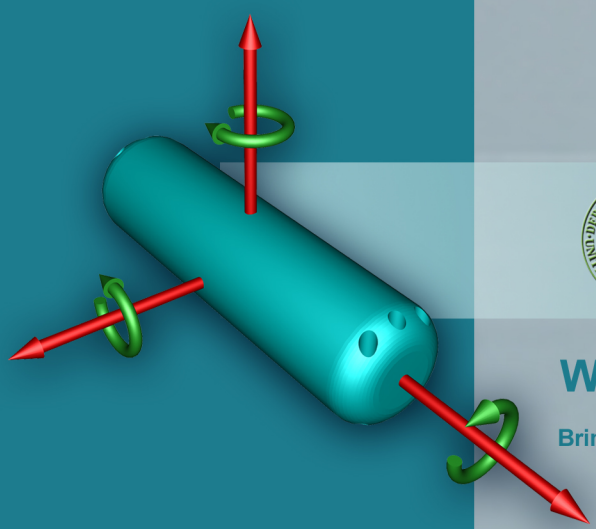

U.S. Department of Energy
Energy Efficiency and Renewable Energy

Wind and Hydropower Technologies

Bringing you a prosperous future where energy is clean, abundant, reliable, and affordable

PACIFIC NORTHWEST NATIONAL LABORATORY
operated by
BATTELLE
for the
UNITED STATES DEPARTMENT OF ENERGY
under Contract DE-AC06-76RLO1830

Printed in the United States of America

Available to DOE and DOE contractors from the
Office of Scientific and Technical Information,
P.O. Box 62, Oak Ridge, TN 37831-0062;
ph: (865) 576-8401
fax: (865) 576-5728
email: reports@adonis.osti.gov

Available to the public from the National Technical Information Service,
U.S. Department of Commerce, 5285 Port Royal Rd., Springfield, VA 22161
ph: (800) 553-6847
fax: (703) 605-6900
email: orders@ntis.fedworld.gov
online ordering: http://www.ntis.gov/ordering.htm


This document was printed on recycled paper.
(8/00)

PNNL-14779

Six-Degree-of-Freedom Sensor Fish Design: Governing Equations and Motion Modeling

Z. Deng
M. C. Richmond
C. S. Simmons
T. J. Carlson

July 2004

Prepared for the U.S. Department of Energy
under Contract DE-AC06-76RL01830

Pacific Northwest National Laboratory
Richland, Washington 99352

Executive Summary

The Sensor Fish device is being used at Northwest hydropower projects to better understand the conditions fish experience during passage through hydroturbines and other dam bypass alternatives. Since its initial development in 1997, the Sensor Fish has undergone numerous design changes to improve its function and extend the range of its use. The most recent Sensor Fish design, the three degree of freedom (3DOF) device, has been used successfully to characterize the environment fish experience when passing through turbines, in spill, or in engineered fish bypass facilities at dams.

Pacific Northwest National Laboratory (PNNL) is in the process of redesigning the current 3DOF Sensor Fish device package to improve its field performance. Rate gyros will be added to the new six degree of freedom (6DOF) device so that it will be possible to observe the six linear and angular accelerations of the Sensor Fish as it passes the dam. Before the 6DOF Sensor Fish device can be developed and deployed, governing equations of motion must be developed in order to understand the design implications of instrument selection and placement within the body of the device.

In this report, we describe a fairly general formulation for the coordinate systems, equations of motion, force and moment relationships necessary to simulate the the 6DOF movement of an underwater body. Some simplifications are made by considering the Sensor Fish device to be a rigid, axisymmetric body. The equations of motion are written in the body-fixed frame of reference. Transformations between the body-fixed and inertial reference frames are performed using a formulation based on quaternions. Force and moment relationships specific to the Sensor Fish body are currently not available. However, examples of the trajectory simulations using the 6DOF equations are presented using existing low and high-Reynolds number force and moment correlations. Animation files for the test cases are provided in an attached CD.

The next phase of the work will focus on the refinement and application of the 6DOF simulator developed in this project. Experimental and computational studies are planned to develop a set of force and moment relationships that are specific to the Sensor Fish body over the range of Reynolds numbers that it experiences. Lab testing of prototype 6DOF Sensor Fish will also allow for refinement of the trajectory simulations through comparison with observations in test flumes. The 6DOF simulator will also be an essential component in tools to analyze field data measured using the next generation Sensor Fish. The 6DOF simulator will be embedded in a moving-machinery computational fluid dynamics (CFD) model for hydroturbines to numerically simulate the 6DOF Sensor Fish.

Acknowledgments

The authors are grateful for the contributions and input of many people on this project. John Serkowski and Bill Perkins provided technical help preparing the manuscript. Georganne O'Connor and Jennifer Zohn were the technical editors for this document. Dennis Dauble's involvement and oversight was also greatly appreciated. Finally, we would like to thank the U.S. Department of Energy's Wind and Hydropower Program for funding this study.

Contents

Figures

1.0 Introduction

Hydropower is a major producer of renewable, non-carbon based, "green" electrical power. However, hydropower production impacts fish that live in or migrate through impounded river systems. In the Pacific Northwest and elsewhere, improvement in the survival and reduction in the injury rate for fish passing through turbines is being sought through changes in hydroturbine design and in hydroturbine operation. An additional goal is production of more electrical power at higher efficiency. Evidence to date indicates these goals are complementary.

The Sensor Fish device (Sensor Fish) is an autonomous device being used to better understand the physical conditions fish experience during passage through hydroturbines and other dam bypass alternatives. Sensor Fish development was initiated at Pacific Northwest National Laboratory in 1997 as an internal development initiative. The product of the initiative was a functional prototype that was field tested in spring 1999 and extensively used during winter 1999-2000 as part of an evaluation of the first minimum gap runner installed at Bonneville Dam's first powerhouse on the Columbia River. The purpose of these field tests was to assess physical damage caused by turbine passage and develop retrieval methods for the Sensor Fish from the tailrace. Since this initial use, the Sensor Fish has undergone numerous design changes to improve its function and extend the range of its use (Carlson et al. 2003; Carlson and Duncan 2003).

The most recent and ambitious extension of function of the Sensor Fish is the current project to add rate gyros to the linear accelerometers which always have been an element of the Sensor Fish package. Adding the rate gyros will permit all six possible motions of the Sensor Fish (three components of linear acceleration plus pitch, roll, and yaw angles) to be observed.

In actual use, the Sensor Fish is only one part of a "system" necessary to acquire data on hydraulic forces. There are other requirements related to deploying and retrieving the Sensor Fish, downloading acquired data, and analyzing and interpreting data. The new Sensor Fish will greatly extend the capabilities of this "system" in many ways. The new sensor package will make it possible for all six degrees of freedom (6DOF) required to describe the motion of a rigid body to be obtained for the Sensor Fish during transit through a hydroturbine or other dam passage route.

The goals of the 6DOF Sensor Fish system project are to:

1. Redesign the 3DOF Sensor Fish to incrementally improve overall Sensor Fish field performance and add rate gyros to provide full 6DOF measurement capability. Some more important design changes include the following:
    - increased analog to digital sampling frequency
    - more non-volatile internal memory for data storage
    - linear accelerometers with increased dynamic range
    - software access to turn the battery on and off and to initiate a charging cycle

- rigid mounting of sensor packages on printed circuit cards
- pressure sensor with smaller external opening and greater sensitivity.

2. Implement a numerical model of the 6DOF Sensor Fish within a particle-tracking module for use with Computational Fluid Dynamics (CFD), moving machinery simulation of hydroturbines.

3. Analyze Sensor Fish data sets and movement simulation software.

In order to achieve these goals, it is first necessary to develop governing equations for the 6DOF motion for a rigid body. The 6DOF equations of motion (6DOF-EOM) described in this report will be used to achieve several critical steps in the design and implementation of the 6DOF Sensor Fish. First, the 6DOF-EOM will be used to evaluate elements of the 6DOF Sensor Fish design. It is essential that the impact on the device motion caused by basic mechanical features of the 6DOF Sensor Fish, particularly the sensor's mass distribution and buoyancy characteristics, are taken into account in the design process.

Second, the 6DOF-EOM will be incorporated into particle-tracking software to numerically simulate the 6DOF Sensor Fish. This approach already has been used. The current 3DOF particle-tracking capability has been used by Richmond et al. (2004) to help analyze and understand 3DOF Sensor Fish data sets and extend analysis of live fish data acquired to assess the biological performance of spill for fish passage at The Dalles Dam.

Third, the 6DOF-EOM will serve as the base of software developed to analyze 6DOF Sensor Fish data sets. Using the 6DOF-EOM in this way will optimize extraction of information for characterizing fish passage conditions from Sensor Fish data sets. In particular, improved data-analysis methods are needed to detect and describe Sensor Fish response to exposure conditions, such as strike, scraping, and shear, events which are the primary injury mechanisms for fish passing through turbines. These developments will permit better use of Sensor Fish data sets and provide improved understanding of the location and dynamics of conditions deleterious to fish during turbine, spill, and bypass passage.

In Section 2 of this report, the equations of motion for an underwater body are written in the body-fixed frame of reference. Section 3 presents force and moment relationships that, while not specifc to the Sensor Fish body, are useful approximations that are used in Section 4 to show examples of the trajectory simulations using the 6DOF equations. Animation files for the test cases are provided in an attached CD.

2.0 Governing Equations of Rigid Body Motion

This chapter defines the coordinate systems and governing equations related to the motion of Sensor Fish. To simplify the derivation of the equations, it is assumed that Sensor Fish are rigid and cylindrical. Therefore, the terms "Sensor Fish" and "rigid body" are interchangeable throughout the report, even though the formulation is general and can be applied to other body shapes such as sphere and ellipsoids.

2.1 Coordinate Systems and Transformations

"Body-fixed coordinate system (frame)" and "inertial coordinate system (frame)" are terms used in this report. The origin of the body-fixed coordinate system is located at the center of buoyancy (center of geometry). Figure 2.1 illustrates the definition of the two systems. There are various ways to describe the general motion of a rigid body in 6DOF. Conventional aerodynamics definitions are used in the current investigation.

Suppose (x, y, z) and (ϕ, θ, ψ) are the position and orientation of Sensor Fish with respect to the inertial coordinate system. In aerodynamics, the Euler angles ϕ, θ and ψ are usually labeled as yaw, pitch, and roll angles, respectively, which can be determined by the following steps: (1) roll angle ψ is obtained by rotating inertial system about its z-axis until its y-axis becomes perpendicular to the plane of the inertial z-axis and the body-fixed x-axis; (2) pitch angle θ is obtained by rotating the new inertial system (created by step 1) about its new y-axis until its x-axis overlaps with the body-fixed x-axis; (3) yaw angle ϕ is finally obtained by continuing to rotate the new inertial system (now created by step

2) about its new x-axis until its y-axis lines up with the body-fixed y-axis. The corresponding homogeneous transformation $\mathbf{A}$ is defined as

$$\begin{aligned}\mathbf{A} &= R(z,\psi)R(y,\theta)R(x,\phi) \\ &= \begin{pmatrix} \cos\theta\cos\psi & \sin\psi\cos\theta & -\sin\theta \\ \cos\psi\sin\theta\sin\phi - \sin\psi\cos\phi & \sin\psi\sin\theta\sin\phi + \cos\psi\cos\phi & \cos\theta\sin\phi \\ \cos\psi\sin\theta\cos\phi + \sin\psi\sin\phi & \sin\psi\sin\theta\cos\phi - \cos\psi\sin\phi & \cos\theta\cos\phi \end{pmatrix}, \quad (2.1)\end{aligned}$$

which is orthogonal and transforms translational velocities between the inertial and body-fixed coordinate systems by

$$\begin{pmatrix} \dot{x} \\ \dot{y} \\ \dot{z} \end{pmatrix} = \mathbf{A}^{-1} \begin{pmatrix} u \\ v \\ w \end{pmatrix} = \mathbf{A}^{T} \begin{pmatrix} u \\ v \\ w \end{pmatrix}, \quad (2.2)$$

where $(u,\ v,\ w)^T$ and $(\dot{x},\ \dot{y},\ \dot{z})^T$ are the translational velocity of Sensor Fish with respect to the body-fixed coordinate system and the inertial system, respectively.

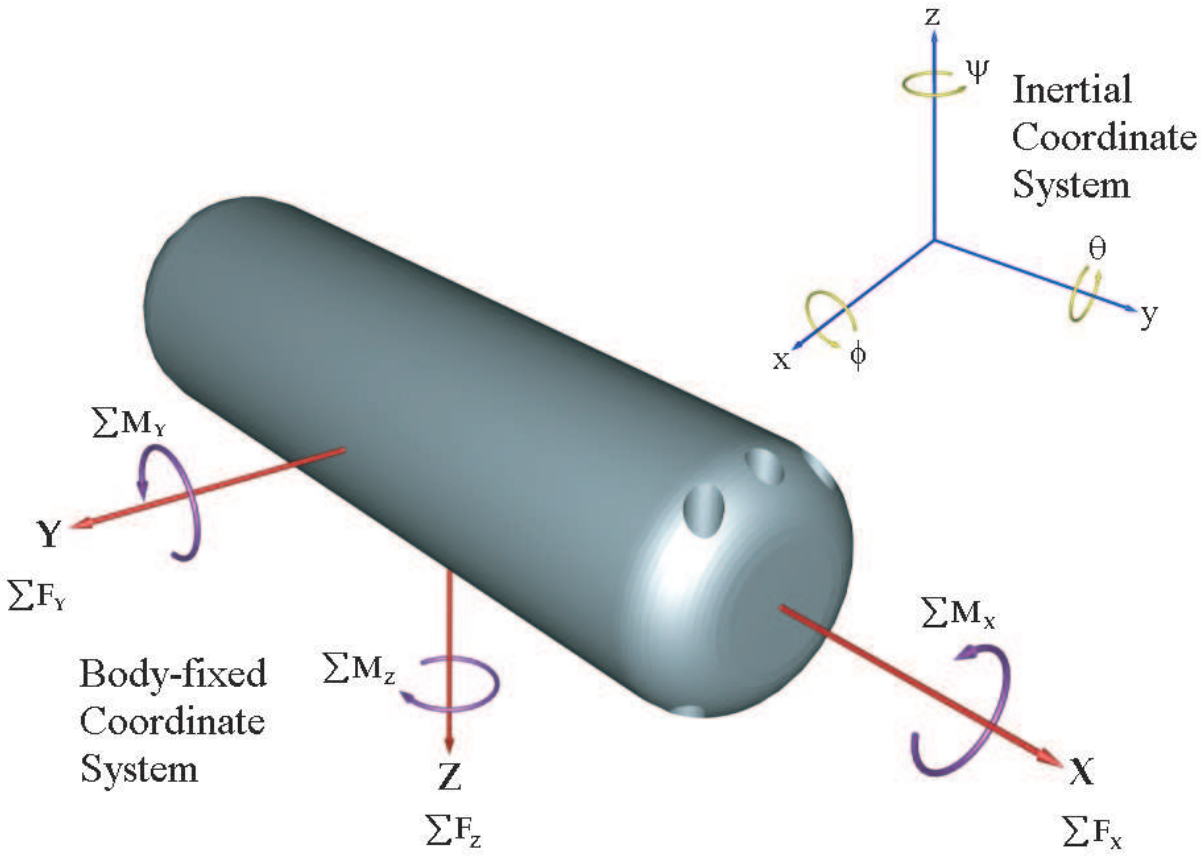

Figure 2.1. Sensor Fish body-fixed and inertial coordinate systems

Components of the angular velocity in the body-fixed system can be expressed in terms of the orientation angles and their derivatives

$$\begin{aligned}\begin{pmatrix} p \\ q \\ r \end{pmatrix} &= \begin{pmatrix} \dot{\phi} - \dot{\psi}\sin\theta \\ \dot{\theta}\cos\phi + \dot{\psi}\sin\phi\cos\theta \\ \dot{\psi}\cos\phi\cos\theta - \dot{\theta}\sin\phi \end{pmatrix} \\ &= \begin{pmatrix} 1 & 0 & -\sin\theta \\ 0 & \cos\phi & \sin\phi\cos\theta \\ 0 & -\sin\phi & \cos\phi\cos\theta \end{pmatrix} \begin{pmatrix} \dot{\phi} \\ \dot{\theta} \\ \dot{\psi} \end{pmatrix}, \end{aligned} \tag{2.3}$$

where $(p,\ q,\ r)^T$ and $(\dot{\phi},\ \dot{\theta},\ \dot{\psi})^T$ are the rotational velocities of Sensor Fish with respect to the body-fixed coordinate system and the inertial system, respectively. Therefore, by computing the inverse of the transformation matrix in Equation (2.3), we can define the transformation matrix of angular velocity, **J**,

$$\begin{pmatrix} \dot{\phi} \\ \dot{\theta} \\ \dot{\psi} \end{pmatrix} = J \begin{pmatrix} p \\ q \\ r \end{pmatrix}, \tag{2.4}$$

where

$$\mathbf{J} = \begin{pmatrix} 1 & \sin\phi\tan\theta & \cos\phi\tan\theta \\ 0 & \cos\phi & -\sin\phi \\ 0 & \sin\phi/\cos\theta & \cos\phi/\cos\theta \end{pmatrix}. \tag{2.5}$$

For the second transformation matrix **J**, there are singularities at $\cos\theta = 0$, that is, when the Sensor Fish has a pitch angle $\theta = \pm 90^\circ$, the coordinate transform based on roll, pitch, and yaw angles doesn't work anymore. This singlarity associated with the use of Euler angles is sometimes referred to as "gimbal-lock". To overcome this deficiency, the quaternion representation for rigid body rotation is introduced.

Let four parameters ε_1, ε_2, ε_3, and ε_4 form the components of the quaternion ε, as follows:

$$\varepsilon = \begin{pmatrix} \varepsilon_1 \\ \varepsilon_2 \\ \varepsilon_3 \\ \varepsilon_4 \end{pmatrix}. \tag{2.6}$$

The general rotation of a rigid body has only three degrees of freedom, so the four components are not independent and satisfy the constraint equation

$$\varepsilon_1^2 + \varepsilon_2^2 + \varepsilon_3^2 + \varepsilon_4^2 = 1. \tag{2.7}$$

The related transformation matrix **Q** in terms of quaternion components is given by

$$\begin{aligned} \mathbf{Q}(\varepsilon) &= \begin{pmatrix} \varepsilon_1^2 - \varepsilon_2^2 - \varepsilon_3^2 + \varepsilon_4^2 & 2(\varepsilon_1\varepsilon_2 + \varepsilon_3\varepsilon_4) & 2(\varepsilon_1\varepsilon_3 - \varepsilon_2\varepsilon_4) \\ 2(\varepsilon_1\varepsilon_2 - \varepsilon_3\varepsilon_4) & -\varepsilon_1^2 + \varepsilon_2^2 - \varepsilon_3^2 + \varepsilon_4^2 & 2(\varepsilon_2\varepsilon_3 + \varepsilon_1\varepsilon_4) \\ 2(\varepsilon_1\varepsilon_3 + \varepsilon_2\varepsilon_4) & 2(\varepsilon_2\varepsilon_3 - \varepsilon_1\varepsilon_4) & -\varepsilon_1^2 - \varepsilon_2^2 + \varepsilon_3^2 + \varepsilon_4^2 \end{pmatrix} \\ &= \begin{pmatrix} 1 - 2(\varepsilon_2^2 + \varepsilon_3^2) & 2(\varepsilon_1\varepsilon_2 + \varepsilon_3\varepsilon_4) & 2(\varepsilon_1\varepsilon_3 - \varepsilon_2\varepsilon_4) \\ 2(\varepsilon_1\varepsilon_2 - \varepsilon_3\varepsilon_4) & 1 - 2(\varepsilon_1^2 + \varepsilon_3^2) & 2(\varepsilon_2\varepsilon_3 + \varepsilon_1\varepsilon_4) \\ 2(\varepsilon_1\varepsilon_3 + \varepsilon_2\varepsilon_4) & 2(\varepsilon_2\varepsilon_3 - \varepsilon_1\varepsilon_4) & 1 - 2(\varepsilon_1^2 + \varepsilon_2^2) \end{pmatrix}. \end{aligned} \tag{2.8}$$

For a given homogeneous transformation matrix **A** as defined in Equation (2.1), quaternion ε can be computed from

$$\mathbf{A} = \mathbf{Q}(\varepsilon_1, \varepsilon_2, \varepsilon_3, \varepsilon_4) \tag{2.9}$$

$$\varepsilon_4 = \pm\frac{1}{2}\sqrt{1 + A_{1,1} + A_{2,2} + A_{3,3}}, \tag{2.10}$$

if $\varepsilon_4 \neq 0$, then

$$\begin{aligned} \varepsilon_1 &= \frac{1}{4\varepsilon_4}(A_{2,3} - A_{3,2}) \\ \varepsilon_2 &= \frac{1}{4\varepsilon_4}(A_{3,1} - A_{1,3}) \\ \varepsilon_3 &= \frac{1}{4\varepsilon_4}(A_{1,2} - A_{2,1}); \end{aligned} \tag{2.11}$$

if $\varepsilon_4 = 0$, then

$$\begin{aligned} \varepsilon_1 &= \frac{1}{2}\sqrt{1+A_{1,1}-A_{2,2}-A_{3,3}} \\ \varepsilon_2 &= \frac{1}{2}\sqrt{1-A_{3,3}-2\varepsilon_1^2} \\ \varepsilon_3 &= \frac{1}{2}\sqrt{1-A_{2,2}-2\varepsilon_1^2}. \end{aligned} \tag{2.12}$$

Note there is a sign ambiguity in the calculation of these components. As a result, there are at least two sets of quaternion parameters. However, the equivalent transformation matrix $\mathbf{Q}(\varepsilon)$ is the same because $\mathbf{Q}(\varepsilon)$ (see Equation [2.8]) is not affected by the simultaneous change of signs of the four components.

The time derivative of the quaternion is related to the rotational velocities in the body-fixed frame,

$$\begin{pmatrix} \dot{\varepsilon}_1 \\ \dot{\varepsilon}_2 \\ \dot{\varepsilon}_3 \\ \dot{\varepsilon}_4 \end{pmatrix} = \begin{pmatrix} d\varepsilon_1/dt \\ d\varepsilon_2/dt \\ d\varepsilon_3/dt \\ d\varepsilon_4/dt \end{pmatrix} = \frac{1}{2}\begin{pmatrix} 0 & r & -q & p \\ -r & 0 & p & q \\ q & -p & 0 & r \\ -p & -q & -r & 0 \end{pmatrix}\begin{pmatrix} \varepsilon_1 \\ \varepsilon_2 \\ \varepsilon_3 \\ \varepsilon_4 \end{pmatrix} \tag{2.13}$$

where t is the time. Refer to Hughes (1986) or Maxey and Riley (1983) for more details of quaternion representation.

On the other hand, for a given quaternion ε, the transformation matrix $\mathbf{Q}(\varepsilon)$ is computed from Equation (2.8), and the related orientation angles can be obtained from

$$\begin{aligned} \theta &= \arcsin(-Q_{1,3}) \\ \phi &= \arctan\frac{Q_{2,3}}{Q_{3,3}} \\ \psi &= \arctan\frac{Q_{1,2}}{Q_{1,1}} \end{aligned} \tag{2.14}$$

2.2 Rigid-Body Dynamics

Because most of the external forces and moments exerted on the Sensor Fish are represented in the body-fixed system, all the governing equations of motion will be written in the body-fixed system as well.

Define

$$\mathbf{v} = \begin{pmatrix} u \\ v \\ w \end{pmatrix}, \ \mathbf{a} = \frac{d\mathbf{v}}{dt} = \begin{pmatrix} \dot{u} \\ \dot{v} \\ \dot{w} \end{pmatrix}, \ \Omega = \begin{pmatrix} p \\ q \\ r \end{pmatrix}, \ \frac{d\Omega}{dt} = \begin{pmatrix} \dot{p} \\ \dot{q} \\ \dot{r} \end{pmatrix}, \tag{2.15}$$

$$\mathbf{r}_g = \begin{pmatrix} x_g \\ y_g \\ z_g \end{pmatrix}, \ \sum\mathbf{F} = \begin{pmatrix} \sum F_X \\ \sum F_Y \\ \sum F_Z \end{pmatrix}, \ \sum\mathbf{M} = \begin{pmatrix} \sum M_X \\ \sum M_Y \\ \sum M_Z \end{pmatrix}, \tag{2.16}$$

where (x_g, y_g, z_g) is the center of mass in the body-fixed frame, that is, the offset of the center of mass with respect to the center of buoyancy because the origin of the body-fixed frame is defined at the center of buoyancy; $\sum \mathbf{F}$ and $\sum \mathbf{M}$ are the total force and moment exerted on the body, and all the components and operations are with respect to the body-fixed frame.

Use vector operation to compute the velocity $\mathbf{v}_g$ and acceleration $\mathbf{a}_g$ at the center of mass in the body-fixed frame, and note that the origin of body-fixed frame is defined at the center of buoyancy,

$$\mathbf{v}_g = \frac{\mathrm{d}\mathbf{r}_g}{\mathrm{d}t} = \mathbf{v} + \Omega \times \mathbf{r}_g, \tag{2.17}$$

then,

$$\begin{aligned} \mathbf{a}_g = \frac{\mathrm{d}\mathbf{v}_g}{\mathrm{d}t} &= \frac{\mathrm{d}}{\mathrm{d}t}(\mathbf{v} + \Omega \times \mathbf{r}_g) \\ &= \frac{\mathrm{d}\mathbf{v}}{\mathrm{d}t} + \frac{\mathrm{d}}{\mathrm{d}t}(\Omega \times \mathbf{r}_g) \\ &= \frac{\mathrm{d}\mathbf{v}}{\mathrm{d}t} + \frac{\mathrm{d}\Omega}{\mathrm{d}t} \times \mathbf{r}_g + \Omega \times \frac{\mathrm{d}\mathbf{r}_g}{\mathrm{d}t} \\ &= \frac{\mathrm{d}\mathbf{v}}{\mathrm{d}t} + \frac{\mathrm{d}\Omega}{\mathrm{d}t} \times \mathbf{r}_g + \Omega \times (\mathbf{v} + \Omega \times \mathbf{r}_g). \end{aligned} \tag{2.18}$$

Use Newton's second law to relate the external forces to linear acceleration,

$$\sum \mathbf{F} = m\,\mathbf{a}_g = m\left(\frac{\mathrm{d}\mathbf{v}}{\mathrm{d}t} + \frac{\mathrm{d}\Omega}{\mathrm{d}t} \times \mathbf{r}_g + \Omega \times \mathbf{v} + \Omega \times (\Omega \times \mathbf{r}_g)\right). \tag{2.19}$$

Similarly, use Euler's equation to relate the external moments to rotational motion of the rigid body,

$$\sum \mathbf{M} = m\,\mathbf{r}_g \times (\frac{\mathrm{d}\mathbf{v}}{\mathrm{d}t} + \Omega \times \mathbf{v}) + \mathbf{I} \cdot \frac{\mathrm{d}\Omega}{\mathrm{d}t} + \Omega \times (\mathbf{I} \cdot \Omega), \tag{2.20}$$

where m is the mass of the rigid body, and

$$\mathbf{I} = \begin{pmatrix} I_{xx} & -I_{xy} & -I_{xz} \\ -I_{xy} & I_{yy} & -I_{yz} \\ -I_{xz} & -I_{yz} & I_{zz} \end{pmatrix} \tag{2.21}$$

is the inertial tensor, in which (I_{xx}, I_{yy}, I_{zz}) are the moments of inertia and the other components are usually referred to as the products of inertia.

Expand Equations (2.19) and (2.20), and obtain the general governing equations of a rigid body

in the body-fixed frame with its origin located at the center of buoyancy:

$$\begin{aligned}
\sum F_X &= m\left[\dot{u}-vr+wq-x_g(q^2+r^2)+y_g(pq-\dot{r})+z_g(pr+\dot{q})\right] \\
\sum F_Y &= m\left[\dot{v}-wp+ur-y_g(p^2+r^2)+z_g(qr-\dot{p})+x_g(pq+\dot{r})\right] \\
\sum F_z &= m\left[\dot{w}-uq+vp-z_g(p^2+q^2)+x_g(pr-\dot{q})+y_g(qr+\dot{p})\right] \\
\sum M_X &= I_{xx}\dot{p}+(I_{zz}-I_{yy})qr-I_{xz}(\dot{r}+pq)+I_{yz}(r^2-q^2)+I_{xy}(pr-\dot{q}) \\
&\quad +m\left[y_g(\dot{w}-uq+vp)-z_g(\dot{v}-wp+ur)\right] \\
\sum M_Y &= I_{yy}\dot{q}+(I_{xx}-I_{zz})pr-I_{xy}(\dot{p}+qr)+I_{zx}(p^2-r^2)+I_{yz}(pq-\dot{r}) \\
&\quad +m\left[z_g(\dot{u}-vr+wq)-x_g(\dot{w}-uq+vp)\right] \\
\sum M_Z &= I_{zz}\dot{r}+(I_{yy}-I_{xx})pq-I_{yz}(\dot{q}+pr)+I_{xy}(q^2-p^2)+I_{xz}(rq-\dot{p}) \\
&\quad +m\left[x_g(\dot{v}-wp+ur)-y_g(\dot{u}-vr+wq)\right]
\end{aligned} \tag{2.22}$$

The governing equations can be re-written in a matrix form,

$$\begin{pmatrix} \sum F_X \\ \sum F_Y \\ \sum F_Z \\ \sum M_X \\ \sum M_Y \\ \sum M_Z \end{pmatrix} = \begin{pmatrix} m & 0 & 0 & 0 & mz_g & -my_g \\ 0 & m & 0 & -mz_g & 0 & mx_g \\ 0 & 0 & m & my_g & -mx_g & 0 \\ 0 & -mz_g & my_g & I_{xx} & -I_{xy} & -I_{xz} \\ mz_g & 0 & -mx_g & -I_{xy} & I_{yy} & -I_{yz} \\ -my_g & mx_g & 0 & -I_{xz} & -I_{yz} & I_{zz} \end{pmatrix} \cdot \begin{pmatrix} \dot{u} \\ \dot{v} \\ \dot{w} \\ \dot{p} \\ \dot{q} \\ \dot{r} \end{pmatrix} +$$

$$\begin{pmatrix} 0 & 0 & 0 & m(z_g r+y_g q) & m(w-x_g q) & -m(v+x_g r) \\ 0 & 0 & 0 & m(w-y_g p) & m(z_g r-y_g q) & m(u-y_g r) \\ 0 & 0 & 0 & -m(v+x_g r) & m(y_g r-u) & -m(x_g p+y_g q) \\ -m(y_g q+z_g r) & m(w+y_g p) & m(z_g p-v) & 0 & I_{zz}r-I_{yz}q-I_{xz}p & I_{yz}r+I_{xx}p-I_{yy}q \\ m(x_g q-w) & -m(z_g r+x_g p) & m(z_g q+u) & I_{yz}q+I_{xz}p+I_{zz}r & 0 & I_{xx}p-I_{xz}r-I_{xy}q \\ m(x_g r+v) & m(y_g r-u) & -m(x_g p+y_g q) & I_{yy}q-I_{xy}p-I_{yz}r & I_{xy}q+I_{xz}r-I_{xx}p & 0 \end{pmatrix} \cdot \begin{pmatrix} u \\ v \\ w \\ p \\ q \\ r \end{pmatrix}$$

Normalize the equations with the mass of the rigid body, get

$$\begin{pmatrix} \sum F'_X \\ \sum F'_Y \\ \sum F'_Z \\ \sum M'_X \\ \sum M'_Y \\ \sum M'_Z \end{pmatrix} = \begin{pmatrix} 1 & 0 & 0 & 0 & z_g & -y_g \\ 0 & 1 & 0 & -z_g & 0 & x_g \\ 0 & 0 & 1 & y_g & -x_g & 0 \\ 0 & -z_g & y_g & I'_{xx} & -I'_{xy} & -I'_{xz} \\ z_g & 0 & -x_g & -I'_{xy} & I'_{yy} & -I'_{yz} \\ -y_g & x_g & 0 & -I'_{xz} & -I'_{yz} & I'_{zz} \end{pmatrix} \cdot \begin{pmatrix} \dot{u} \\ \dot{v} \\ \dot{w} \\ \dot{p} \\ \dot{q} \\ \dot{r} \end{pmatrix} +$$

$$\begin{pmatrix} 0 & 0 & 0 & (z_g r+y_g q) & (w-x_g q) & -(v+x_g r) \\ 0 & 0 & 0 & (w-y_g p) & (z_g r-y_g q) & (u-y_g r) \\ 0 & 0 & 0 & -(v+x_g r) & (y_g r-u) & -(x_g p+y_g q) \\ -(y_g q+z_g r) & (w+y_g p) & (z_g p-v) & 0 & I'_{zz}r-I'_{yz}q-I'_{xz}p & I'_{yz}r+I'_{xx}p-I'_{yy}q \\ (x_g q-w) & -(z_g r+x_g p) & (z_g q+u) & I'_{yz}q+I'_{xz}p+I'_{zz}r & 0 & I'_{xx}p-I'_{xz}r-I'_{xy}q \\ (x_g r+v) & (y_g r-u) & -(x_g p+y_g q) & I'_{yy}q-I'_{xy}p-I'_{yz}r & I'_{xy}q+I'_{xz}r-I'_{xx}p & 0 \end{pmatrix} \cdot \begin{pmatrix} u \\ v \\ w \\ p \\ q \\ r \end{pmatrix}$$

where

$$\begin{pmatrix} \sum F'_X \\ \sum F'_Y \\ \sum F'_Z \\ \sum M'_X \\ \sum M'_Y \\ \sum M'_Z \end{pmatrix} = \begin{pmatrix} \sum F_X/m \\ \sum F_Y/m \\ \sum F_Z/m \\ \sum M_X/m \\ \sum M_Y/m \\ \sum M_Z/m \end{pmatrix} \tag{2.23}$$

and

$$\mathbf{I}' = \begin{pmatrix} I'_{xx} & -I'_{xy} & -I'_{xz} \\ -I'_{xy} & I'_{yy} & -I'_{yz} \\ -I'_{xz} & -I'_{yz} & I'_{zz} \end{pmatrix} = \mathbf{I}/m = \begin{pmatrix} I_{xx}/m & -I_{xy}/m & -I_{xz}/m \\ -I_{xy}/m & I_{yy}/m & -I_{yz}/m \\ -I_{xz}/m & -I_{yz}/m & I_{zz}/m \end{pmatrix} \tag{2.24}$$

3.0 Forces and Coefficients Evaluation

For the equations of a rigid-body motion in a water flow field, the total forces and moments are

$$\begin{aligned} \sum \mathbf{F} &= \mathbf{F_{HS}} + \mathbf{F_L} + \mathbf{F_D} + \mathbf{F_A} + \mathbf{F_P} \\ \sum \mathbf{M} &= \mathbf{M_{HS}} + \mathbf{M_L} + \mathbf{M_D} + \mathbf{M_A} + \mathbf{M_P} \end{aligned} \tag{3.1}$$

where $\mathbf{F_{HS}}$ and $\mathbf{M_{HS}}$ are hydrostatic forces and moments, $\mathbf{F_L}$ and $\mathbf{M_L}$ are body lift forces and moments, $\mathbf{F_D}$ and $\mathbf{M_D}$ are body hydrodynamic drag forces and moments, $\mathbf{F_A}$ and $\mathbf{M_A}$ are the corresponding forces and moments of added mass, and $\mathbf{F_P}$ and $\mathbf{M_P}$ are propulsion forces and moments.

In the current investigation, no propulsion is assumed, i.e., $\mathbf{M_P} = \mathbf{0}$, $\mathbf{F_P} = \mathbf{0}$, so Equation (3.1) becomes

$$\begin{aligned} \sum \mathbf{F} &= \mathbf{F_{HS}} + \mathbf{F_L} + \mathbf{F_D} + \mathbf{F_A} \\ \sum \mathbf{M} &= \mathbf{M_{HS}} + \mathbf{M_L} + \mathbf{M_D} + \mathbf{M_A} \end{aligned} \tag{3.2}$$

3.1 Flow Field

Suppose the ambient flow field has velocity (V_x, V_y, V_z) in the inertial frame; then the angular velocity is defined as

$$\begin{aligned} \omega_x &= \tfrac{1}{2}\left(\frac{\partial V_z}{\partial y} - \frac{\partial V_y}{\partial z}\right) \\ \omega_y &= \tfrac{1}{2}\left(\frac{\partial V_x}{\partial z} - \frac{\partial V_z}{\partial x}\right) \\ \omega_z &= \tfrac{1}{2}\left(\frac{\partial V_y}{\partial x} - \frac{\partial V_x}{\partial y}\right) \end{aligned} \tag{3.3}$$

In the body-fixed frame they are transformed to

$$\begin{aligned} \begin{pmatrix} V_1(\varepsilon) \\ V_2(\varepsilon) \\ V_3(\varepsilon) \end{pmatrix} &= \mathbf{Q}(\varepsilon) \cdot \begin{pmatrix} V_x \\ V_y \\ V_z \end{pmatrix} \\ &= \begin{pmatrix} V_x Q_{1,1}(\varepsilon) + V_y Q_{1,2}(\varepsilon) + V_z Q_{1,3}(\varepsilon) \\ V_x Q_{2,1}(\varepsilon) + V_y Q_{2,2}(\varepsilon) + V_z Q_{2,3}(\varepsilon) \\ V_x Q_{3,1}(\varepsilon) + V_y Q_{3,2}(\varepsilon) + V_z Q_{3,3}(\varepsilon) \end{pmatrix} \end{aligned} \tag{3.4}$$

$$\begin{aligned} \begin{pmatrix} \omega_1(\varepsilon) \\ \omega_2(\varepsilon) \\ \omega_3(\varepsilon) \end{pmatrix} &= \mathbf{Q}(\varepsilon) \cdot \begin{pmatrix} \omega_x \\ \omega_y \\ \omega_z \end{pmatrix} \\ &= \begin{pmatrix} \omega_x Q_{1,1}(\varepsilon) + \omega_y Q_{1,2}(\varepsilon) + \omega_z Q_{1,3}(\varepsilon) \\ \omega_x Q_{2,1}(\varepsilon) + \omega_y Q_{2,2}(\varepsilon) + \omega_z Q_{2,3}(\varepsilon) \\ \omega_x Q_{3,1}(\varepsilon) + \omega_y Q_{3,2}(\varepsilon) + \omega_z Q_{3,3}(\varepsilon) \end{pmatrix} \end{aligned} \tag{3.5}$$

where $\begin{pmatrix} V_1(\varepsilon) \\ V_2(\varepsilon) \\ V_3(\varepsilon) \end{pmatrix}$ and $\begin{pmatrix} \omega_1(\varepsilon) \\ \omega_2(\varepsilon) \\ \omega_3(\varepsilon) \end{pmatrix}$ are the translational velocity and angular velocity of the ambient flow field in the body-fixed frame.

Define gradient tensor of the ambient velocity in the inertial frame,

$$\nabla \mathbf{V_e} = \begin{pmatrix} \frac{\partial Vx}{\partial x} & \frac{\partial Vx}{\partial y} & \frac{\partial Vx}{\partial z} \\ \frac{\partial Vy}{\partial x} & \frac{\partial Vy}{\partial y} & \frac{\partial Vy}{\partial z} \\ \frac{\partial Vz}{\partial x} & \frac{\partial Vz}{\partial y} & \frac{\partial Vz}{\partial z} \end{pmatrix} \tag{3.6}$$

and in the body-fixed frame, it becomes

$$\nabla \mathbf{V_b} = \mathbf{Q} \cdot (\nabla \mathbf{V_e}) \cdot \mathbf{Q^{-1}} \tag{3.7}$$

where the subscripts b and e relate to the body-fixed frame and the earth-fixed (inertial) frame, respectively.

The time derivative of the transformation matrix $\mathbf{Q}$ is

$$\dot{Q}_{i,j} = \frac{\partial Q_{i,j}}{\partial \varepsilon_1}\dot{\varepsilon}_1 + \frac{\partial Q_{i,j}}{\partial \varepsilon_2}\dot{\varepsilon}_2 + \frac{\partial Q_{i,j}}{\partial \varepsilon_3}\dot{\varepsilon}_3 + \frac{\partial Q_{i,j}}{\partial \varepsilon_4}\dot{\varepsilon}_4, \quad i,j = 1,2,3 \tag{3.8}$$

where

$$\begin{pmatrix} \dot{\varepsilon}_1 \\ \dot{\varepsilon}_2 \\ \dot{\varepsilon}_3 \\ \dot{\varepsilon}_4 \end{pmatrix} = \frac{1}{2} \begin{pmatrix} 0 & r & -q & p \\ -r & 0 & p & q \\ q & -p & 0 & r \\ -p & -q & -r & 0 \end{pmatrix} \begin{pmatrix} \varepsilon_1 \\ \varepsilon_2 \\ \varepsilon_3 \\ \varepsilon_4 \end{pmatrix} \tag{3.9}$$

Now evaluate the acceleration of the flow velocity in the body-fixed frame,

$$\begin{aligned} \begin{pmatrix} \dot{V}_1 \\ \dot{V}_2 \\ \dot{V}_3 \end{pmatrix} &= \mathbf{Q} \cdot \begin{pmatrix} \dot{V}_x \\ \dot{V}_y \\ \dot{V}_z \end{pmatrix} + \dot{\mathbf{Q}} \cdot \begin{pmatrix} V_x \\ V_y \\ V_z \end{pmatrix} \\ &= \mathbf{Q} \cdot \left[\nabla \mathbf{V_e} \cdot \begin{pmatrix} \dot{x} \\ \dot{y} \\ \dot{z} \end{pmatrix} + \frac{\partial}{\partial t} \begin{pmatrix} V_x \\ V_y \\ V_z \end{pmatrix} \right] + \dot{\mathbf{Q}} \cdot \begin{pmatrix} V_x \\ V_y \\ V_z \end{pmatrix} \\ &= \mathbf{Q} \cdot (\nabla \mathbf{V_e}) \cdot \mathbf{Q}^{-1} \cdot \begin{pmatrix} u \\ v \\ w \end{pmatrix} + \mathbf{Q} \cdot \frac{\partial}{\partial t} \begin{pmatrix} V_x \\ V_y \\ V_z \end{pmatrix} + \dot{\mathbf{Q}} \cdot \begin{pmatrix} V_x \\ V_y \\ V_z \end{pmatrix} \qquad (3.10) \\ &= \nabla \mathbf{V_b} \cdot \begin{pmatrix} u \\ v \\ w \end{pmatrix} + \mathbf{Q} \cdot \frac{\partial}{\partial t} \begin{pmatrix} V_x \\ V_y \\ V_z \end{pmatrix} + \dot{\mathbf{Q}} \cdot \begin{pmatrix} V_x \\ V_y \\ V_z \end{pmatrix} \qquad (3.11) \end{aligned}$$

Computing the rate of change of the flow angular velocity in the body-fixed frame requires differentiating $\nabla \mathbf{V_b}$ with respect to time. This will also require introducing second order spatial

partial derivatives of the flow velocity in the inertial frame. The time derivative is

$$\frac{\mathrm{d}\nabla\mathbf{V_b}}{\mathrm{d}t} = \dot{\mathbf{Q}}\cdot\nabla\mathbf{V_e}\cdot\mathbf{Q}^{-1} + \mathbf{Q}\cdot\frac{\mathrm{d}\nabla\mathbf{V_e}}{\mathrm{d}t}\cdot\mathbf{Q}^{-1} + \mathbf{Q}\cdot\nabla\mathbf{V_e}\cdot(\dot{\mathbf{Q}})^{-1} \tag{3.12}$$

where

$$\frac{\mathrm{d}\nabla\mathbf{V_e}}{\mathrm{d}t} = \left(\frac{\partial\nabla\mathbf{V_e}}{\partial x}, \frac{\partial\nabla\mathbf{V_e}}{\partial y}, \frac{\partial\nabla\mathbf{V_e}}{\partial z}\right)\cdot\begin{pmatrix}\dot{x}\\ \dot{y}\\ \dot{z}\end{pmatrix} + \frac{\partial\nabla\mathbf{V_e}}{\partial t} \tag{3.13}$$

Finally, the rate of change of the ambient angular velocity in the body-fixed frame is obtained as follows:

$$\begin{aligned}
\dot{\omega}_1 &= \frac{1}{2}\left(\frac{\mathrm{d}(\nabla\mathbf{V_b})_{r,q}}{\mathrm{d}t} - \frac{\mathrm{d}(\nabla\mathbf{V_b})_{q,r}}{\mathrm{d}t}\right)\\
\dot{\omega}_2 &= \frac{1}{2}\left(\frac{\mathrm{d}(\nabla\mathbf{V_b})_{p,r}}{\mathrm{d}t} - \frac{\mathrm{d}(\nabla\mathbf{V_b})_{r,p}}{\mathrm{d}t}\right)\\
\dot{\omega}_3 &= \frac{1}{2}\left(\frac{\mathrm{d}(\nabla\mathbf{V_b})_{q,p}}{\mathrm{d}t} - \frac{\mathrm{d}(\nabla\mathbf{V_b})_{p,q}}{\mathrm{d}t}\right)
\end{aligned} \tag{3.14}$$

3.2 Hydrostatics

Hydrostatic forces include body weight (W) and buoyancy (B). In the inertial frame,

$$\mathbf{W} = \begin{pmatrix}0\\0\\W\end{pmatrix}, \mathbf{B} = \begin{pmatrix}0\\0\\B\end{pmatrix} \tag{3.15}$$

Note the governing equations are with respect to body-fixed coordinate system and by applying the quaternion transformation matrix defined in Equation (2.8), express the hydrostatic forces and moments in the body-fixed frame as

$$\mathbf{W}(\varepsilon) = \mathbf{Q}(\varepsilon)\cdot\begin{pmatrix}0\\0\\W\end{pmatrix}, \quad \mathbf{B}(\varepsilon) = \mathbf{Q}(\varepsilon)\cdot\begin{pmatrix}0\\0\\B\end{pmatrix} \tag{3.16}$$

$$\mathbf{F_{HS}}(\varepsilon) = \begin{pmatrix}X_{HS}(\varepsilon)\\Y_{HS}(\varepsilon)\\Z_{HS}(\varepsilon)\end{pmatrix} = \mathbf{W}(\varepsilon) - \mathbf{B}(\varepsilon) = \begin{pmatrix}(W-B)Q_{1,3}(\varepsilon)\\(W-B)Q_{2,3}(\varepsilon)\\(W-B)Q_{3,3}(\varepsilon)\end{pmatrix} \tag{3.17}$$

$$\begin{aligned}
\mathbf{M_{HS}}(\varepsilon) &= \begin{pmatrix}K_{HS}(\varepsilon)\\M_{HS}(\varepsilon)\\N_{HS}(\varepsilon)\end{pmatrix} = \begin{pmatrix}x_g\\y_g\\z_g\end{pmatrix}\times\mathbf{W}(\varepsilon) - \begin{pmatrix}x_b\\y_b\\z_b\end{pmatrix}\times\mathbf{B}(\varepsilon)\\
&= \begin{pmatrix}(y_gW - y_bB)Q_{3,3}(\varepsilon) - (z_gW - z_bB)Q_{2,3}(\varepsilon)\\(z_gW - z_bB)Q_{1,3}(\varepsilon) - (x_gW - x_bB)Q_{3,3}(\varepsilon)\\(x_gW - x_bB)Q_{2,3}(\varepsilon) - (y_gW - y_bB)Q_{1,3}(\varepsilon)\end{pmatrix}
\end{aligned} \tag{3.18}$$

where (x_b, y_b, z_b) is the center of buoyancy in the body-fixed frame.

As defined earlier, the origin of body-fixed coordinate system is at the center of buoyancy, that is, $x_b = y_b = z_b = 0$, so the final expressions for hydrostatic forces and moments are

$$\begin{pmatrix} \mathbf{F_{HS}}(\varepsilon) \\ \mathbf{M_{HS}}(\varepsilon) \end{pmatrix} = \begin{pmatrix} X_{HS}(\varepsilon) \\ Y_{HS}(\varepsilon) \\ Z_{HS}(\varepsilon) \\ K_{HS}(\varepsilon) \\ M_{HS}(\varepsilon) \\ N_{HS}(\varepsilon) \end{pmatrix} = \begin{pmatrix} (W-B)Q_{1,3}(\varepsilon) \\ (W-B)Q_{2,3}(\varepsilon) \\ (W-B)Q_{3,3}(\varepsilon) \\ y_g W Q_{3,3}(\varepsilon) - z_g W Q_{2,3}(\varepsilon) \\ z_g W Q_{1,3}(\varepsilon) - x_g W Q_{3,3}(\varepsilon) \\ x_g W Q_{2,3}(\varepsilon) - y_g W Q_{1,3}(\varepsilon) \end{pmatrix} \tag{3.19}$$

3.3 Added Mass

When a rigid body accelerates within a fluid field, some amount of surrounding fluid moves with the body. Added mass is a measure of this moving fluid and relates the linear and angular acceleration to the hydrodynamics forces exerted by the moving fluid. As noted by Mougin and Magnaudet (2002) added-mass effects are independent of Reynolds number and whether the flow is steady or unsteady. Newman (1977) derived the forces and moments for ideal fluid due to the added mass in a stationary flow field,

$$\begin{aligned} (F_A)_j &= -\dot{\tilde{v}}_i m_{ji} - \varepsilon_{jkl}\tilde{v}_i \Omega_k m_{li} \\ (M_A)_j &= -\dot{\tilde{v}}_i m_{j+3,i} - \varepsilon_{jkl}\tilde{v}_i \Omega_k m_{l+3,i} - \varepsilon_{jkl}\tilde{v}_k \tilde{v}_i m_{li} \\ i &= 1,2,3,4,5,6 \\ j,k,l &= 1,2,3 \end{aligned} \tag{3.20}$$

where ε_{jkl} is the alternating tensor which is equal to 1 when the indices form an even permutation of (123), -1 when the indices form an odd permutation of (123), and zero if any two of the indices are equal; j, k, and l are the dummy indices as defined in summation convention (Einstein Convention); m_{ij} is the 6×6 added mass coefficients tensor; Ω_k is the angular velocity vector of Sensor Fish with respect to the body-fixed frame; $\tilde{v}_i$ is the redundant notation of six velocity components, defined as

$$\tilde{\mathbf{v}} = \begin{pmatrix} \mathbf{v} \\ \Omega \end{pmatrix} = \begin{pmatrix} u \\ v \\ w \\ p \\ q \\ r \end{pmatrix} \quad \text{and} \quad \dot{\tilde{\mathbf{v}}} = \frac{\mathrm{d}\tilde{\mathbf{v}}}{\mathrm{d}t} = \begin{pmatrix} \dot{u} \\ \dot{v} \\ \dot{w} \\ \dot{p} \\ \dot{q} \\ \dot{r} \end{pmatrix} \tag{3.21}$$

For a cylinder or ellipsoid, due to its symmetry, the added mass coefficients tensor m_{ij} becomes

$$m_{ij} = \begin{pmatrix} m_{1,1} & 0 & 0 & 0 & 0 & 0 \\ 0 & m_{2,2} & 0 & 0 & 0 & m_{2,6} \\ 0 & 0 & m_{3,3} & 0 & m_{3,5} & 0 \\ 0 & 0 & 0 & m_{4,4} & 0 & 0 \\ 0 & 0 & m_{5,3} & 0 & m_{5,5} & 0 \\ 0 & m_{6,2} & 0 & 0 & 0 & m_{6,6} \end{pmatrix} \tag{3.22}$$

where $m_{2,2} = m_{3,3}$; $m_{5,5} = m_{6,6}$; $m_{2,6} = m_{6,2}$; $m_{3,5} = m_{5,3}$; $m_{2,6} = -m_{5,3}$.

Re-define the the nontrivial components in order to better relate to the forces and moments due to the added mass,

$$m_{ij} = -\begin{pmatrix} X_{A\dot{u}} & 0 & 0 & 0 & 0 & 0 \\ 0 & Y_{A\dot{v}} & 0 & 0 & 0 & N_{A\dot{v}} \\ 0 & 0 & Z_{A\dot{w}} & 0 & M_{A\dot{w}} & 0 \\ 0 & 0 & 0 & K_{A\dot{p}} & 0 & 0 \\ 0 & 0 & Z_{A\dot{q}} & 0 & M_{A\dot{q}} & 0 \\ 0 & Y_{A\dot{r}} & 0 & 0 & 0 & N_{A\dot{r}} \end{pmatrix} \tag{3.23}$$

Substituting Equation (3.23) into Equation (3.20) results in simplified expressions for forces and moments induced by the added mass.

$$\begin{pmatrix} \mathbf{F_A} \\ \mathbf{M_A} \end{pmatrix} = \begin{pmatrix} X_A \\ Y_A \\ Z_A \\ K_A \\ M_A \\ N_A \end{pmatrix} = \begin{pmatrix} X_{A\dot{u}}\dot{u} + Z_{A\dot{w}}wq + Z_{A\dot{q}}q^2 - Y_{A\dot{v}}vr - Y_{A\dot{r}}r^2 \\ Y_{A\dot{v}}\dot{v} + Y_{A\dot{r}}\dot{r} + X_{A\dot{u}}ur - Z_{A\dot{w}}wp - Z_{A\dot{q}}pq \\ Z_{A\dot{w}}\dot{w} + Z_{A\dot{q}}\dot{q} - X_{A\dot{u}}uq + Y_{A\dot{v}}vp + Y_{A\dot{r}}rp \\ K_{A\dot{p}}\dot{p} \\ M_{A\dot{w}}\dot{w} + M_{A\dot{q}}\dot{q} - (Z_{A\dot{w}} - X_{A\dot{u}})uw - Y_{A\dot{r}}vp + (K_{A\dot{p}} - N_{A\dot{r}})rp - Z_{A\dot{q}}uq \\ N_{A\dot{v}}\dot{v} + N_{A\dot{r}}\dot{r} - (X_{A\dot{u}} - Y_{A\dot{v}})uv + Z_{A\dot{q}}wp - (K_{A\dot{p}} - M_{A\dot{q}})pq + Y_{A\dot{r}}ur \end{pmatrix} \tag{3.24}$$

The axial added mass can be estimated by approximating the rigid body as an ellipsoid. An empirical formula was given by Blevins (1993),

$$X_{A\dot{u}} = -\frac{4\alpha\rho\pi}{3}\left(\frac{L}{2}\right)^2\left(\frac{d}{2}\right)^2 \tag{3.25}$$

where α is an empirical parameter based on the ratio of the body length and diameter.

Newman (1977) computed the added mass on a rigid-body using strip theory and defined the added mass per unit length of a single cylindrical slice

$$m_a(x) = \pi\rho R(x)^2, \tag{3.26}$$

where $R(x)$ is the radius along body-fixed axial position.

The cross-flow added mass terms can be obtained by integrating Equation (3.26) from forward

position (x_f) to tail position (x_t) of the rigid body:

$$\begin{aligned}
Y_{A\dot{v}} &= -m_{2,2} = -\int_{x_t}^{x_f} m_a(x)dx \\
Z_{A\dot{w}} &= -m_{3,3} = -m_{2,2} = Y_{A\dot{v}} \\
M_{A\dot{w}} &= -m_{3,5} = \int_{x_t}^{x_f} x\, m_a(x)dx \\
N_{A\dot{v}} &= -m_{2,6} = m_{3,5} = -M_{A\dot{w}} \\
Y_{A\dot{r}} &= -m_{6,2} = -m_{2,6} = N_{A\dot{v}} \\
Z_{A\dot{q}} &= -m_{5,3} = -m_{3,5} = M_{A\dot{w}} \\
M_{A\dot{q}} &= -m_{5,5} = -\int_{x_t}^{x_f} x^2\, m_a(x)dx \\
N_{A\dot{r}} &= -m_{6,6} = -m_{5,5} = M_{A\dot{q}}
\end{aligned} \tag{3.27}$$

In the current investigation, Sensor Fish is assumed to be cylindrical, and

$$m_a(x) = d/2, \quad x_f = -L/2, \quad x_t = L/2, \tag{3.28}$$

from Equation (3.27), we have

$$m_{2,6} = m_{6,2} = m_{3,5} = m_{5,3} = 0, \tag{3.29}$$

and m_{ij} is reduced into a diagonal matrix. Equation (3.29) also holds for an ellipsoid because $m_a(x) = m_a(-x)$ and $x_t = -x_f$.

Rolling added mass is acquired empirically. From Blevins (1993),

$$K_{A\dot{p}} = -\int_{x_t}^{x_f} \frac{2\rho}{\pi}\left(\frac{d}{2}\right)^4 dx. \tag{3.30}$$

Define cross-terms,

$$\begin{array}{cccc}
X_{Awq} = Z_{A\dot{w}}, & X_{Aqq} = Z_{A\dot{q}}, & X_{Avr} = -Y_{A\dot{v}}, & X_{Arr} = -Y_{A\dot{r}} \\
Y_{Aur} = X_{A\dot{u}}, & Y_{Awp} = -Z_{A\dot{w}}, & Y_{Apq} = -Z_{A\dot{q}} & \\
Z_{Auq} = -X_{A\dot{u}}, & Z_{Avp} = Y_{A\dot{v}}, & Z_{Arp} = Y_{A\dot{r}} & \\
M_{Auw} = -(Z_{A\dot{w}} - X_{A\dot{u}}), & M_{Avp} = -Y_{A\dot{r}}, & M_{Arp} = (K_{A\dot{p}} - N_{A\dot{r}}), & M_{Auq} = -Z_{A\dot{q}} \\
N_{Auv} = -(X_{A\dot{u}} - Y_{A\dot{v}}), & N_{Awp} = Z_{A\dot{q}}, & N_{Apq} = -(K_{A\dot{p}} - M_{A\dot{q}}), & N_{Aur} = Y_{A\dot{r}}
\end{array} \tag{3.31}$$

where M_{Auw} and N_{Auv} represent the pure moment exerted on the body in an inviscid flow at an attach angle and are usually known as Munk Moment in marine hydrodynamics.

Substitute Equation (3.31) into Equation (3.24), and get the equation of the added mass for a rigid body in a stationary flow field:

$$\begin{pmatrix} \mathbf{F_A} \\ \mathbf{M_A} \end{pmatrix} = \begin{pmatrix} X_A \\ Y_A \\ Z_A \\ K_A \\ M_A \\ N_{AA} \end{pmatrix} = \begin{pmatrix} X_{A\dot{u}}\dot{u} + X_{Awq}wq + X_{Aqq}q^2 + X_{Avr}vr + X_{Arr}r^2 \\ Y_{A\dot{v}}\dot{v} + Y_{A\dot{r}}\dot{r} + Y_{Aur}ur + Y_{Awp}wp + Y_{Apq}pq \\ Z_{A\dot{w}}\dot{w} + Z_{A\dot{q}}\dot{q} + Z_{Auq}uq + Z_{Avp}vp + Z_{Arp}rp \\ K_{A\dot{p}}\dot{p} \\ M_{A\dot{w}}\dot{w} + M_{A\dot{q}}\dot{q} + M_{Auw}uw + M_{Avp}vp + M_{Arp}rp + M_{Auq}uq \\ N_{A\dot{v}}\dot{v} + N_{A\dot{r}}\dot{r} + N_{Auv}uv + N_{Awp}wp + N_{Apq}pq + N_{Aur}ur \end{pmatrix} \tag{3.32}$$

Take the ambient flow field into account, and obtain the final expressions for added mass:

$$\begin{pmatrix} \mathbf{F_A} \\ \mathbf{M_A} \end{pmatrix} = \begin{pmatrix} X_A & Y_A & Z_A & K_A & M_A & N_A \end{pmatrix}^T$$

$$\begin{aligned}
X_A &= X_{A\dot{u}}(\dot{u}-\dot{V}_1) + X_{Awq}(w-V_3)(q-\omega_2) + X_{Aqq}(q-\omega_2)^2 + X_{Avr}(v-V_2)(r-\omega_3) + X_{Arr}(r-\omega_3)^2 \\
Y_A &= Y_{A\dot{v}}(\dot{v}-\dot{V}_2) + Y_{A\dot{r}}(\dot{r}-\dot{\omega}_3) + Y_{Aur}(u-V_1)(r-\omega_3) + Y_{Awp}(w-V_3)(p-\omega_1) + Y_{Apq}(p-\omega_1)(q-\omega_2) \\
Z_A &= Z_{A\dot{w}}(\dot{w}-\dot{V}_3) + Z_{A\dot{q}}(\dot{q}-\dot{\omega}_2) + Z_{Auq}(u-V_1)(q-\omega_2) + Z_{Avp}(v-V_2)(p-\omega_1) + Z_{Arp}(r-\omega_3)(p-\omega_1) \\
K_A &= K_{A\dot{p}}(\dot{p}-\dot{\omega}_1) \\
M_A &= M_{A\dot{w}}(\dot{w}-\dot{V}_3) + M_{A\dot{q}}(\dot{q}-\dot{\omega}_2) + M_{Auw}(u-V_1)(w-V_3) + \\
&\quad M_{Avp}(v-V_2)(p-\omega_1) + M_{Arp}(r-\omega_3)(p-\omega_1) + M_{Auq}(u-V_1)(q-\omega_2) \\
N_A &= N_{A\dot{v}}(\dot{v}-\dot{V}_2) + N_{A\dot{r}}(\dot{r}-\dot{\omega}_3) + N_{Auv}(u-V_1)(v-V_2) + N_{Awp}(w-V_3)(p-\omega_1) + \\
&\quad N_{Apq}(p-\omega_1)(q-\omega_2) + N_{Aur}(u-V_1)(r-\omega_3)
\end{aligned} \tag{3.33}$$

3.4 Drag Forces and Moments

In general, the hydrodynamics damping forces and moments acting on an underwater moving rigid body are highly nonlinear and coupled (Fossen 1994). Because the principal component is skin friction due to the existence of the boundary layer on the body surface (Conte and Serrani 1996), only viscous drag is taken into account. In addition, due to the highly non-linear nature of hydrodynamics damping, only linear viscous effects are considered, and all damping terms higher than second-order are neglected.

Reynolds number Re is defined as

$$\mathrm{Re} = \frac{U_{slip} L}{\nu} \tag{3.34}$$

where U_{slip} is the slip velocity of the rigid body, L is the length, and ν is kinematic viscosity of water. For a typical case of Sensor Fish, let $L = 10\ cm$, $U_{slip} = 10\ m/s$, and $\nu = 1.004 \times 10^{-6}$ m^2/s, then $\mathrm{Re} = 10^6$, which falls in the turbulent regime.

Unless pointed out specifically, the following formulation for drag and lift coefficients applies to high Reynolds numbers, i.e., turbulent regime. Low Reynolds number hydrodynamics was examined by Happel and Brenner (1983) and the corresponding motion of equations of an ellipsoid is derived separately in Section 4.3.2 and Appendix A. In addition, because there are no analytical solutions for turbulent flows, empirical formulae are generally used.

3.4.1 Axial Drag Coefficients

For axial drag, from Hoerner (1965),

$$X_{Duu} = -(\frac{1}{2}\rho C_D A_f) \tag{3.35}$$

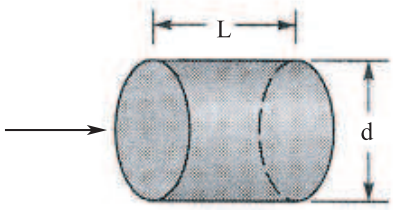

L/d	C_D
0.5	1.1
1.0	0.93
2.0	0.83
4.0	0.85

Table 3.1. Typical drag coefficients for cylinder parallel to flow at Re $> 10^5$

$$X_D = X_{Duu}(u-V_1)|u-V_1| = -(\frac{1}{2}\rho C_D A_f)(u-V_1)|u-V_1| \tag{3.36}$$

where A_f is the front area of the rigid body, ρ is the density of water, and C_D is the axial drag coefficient. C_D is obtained by either direct experimental measurement or empirical estimation,

$$C_D = \frac{c_{ss}\pi A_p}{A_f}(1+60(\frac{d}{L})^3+0.0025(\frac{L}{d})^2)) \tag{3.37}$$

where c_{ss} is the Schoenherr's value, A_p is the projected area of the rigid body, and d is the diameter.

Prestero (2001) found that the empirical formula (Equation [3.37]) underestimates the magnitude of drag coefficient compared with experimental results. In his simulation of an underwater vehicle, C_D was doubled to be comparable with direct experimental measurement.

In this study, a straightforward approach is taken due to the relatively simplicity of the shape of Sensor Fish and availability of empirical data. Table 3.1 is adapted from Munson et al. (1999) and lists the axial drag coefficient of a cylinder with different configurations for Re $> 10^5$.

3.4.2 Cross-Flow Drag Coefficients

Apply slender body theory used for calculating added mass to estimate cross-flow drag coefficients,

$$\begin{aligned}
Y_{Dvv} &= Z_{Dww} &&= -\frac{1}{2}\rho c_{dc}\int_{x_t}^{x_f} 2R(x)dx \\
M_{Dww} &= -N_{Dvv} &&= \frac{1}{2}\rho c_{dc}\int_{x_t}^{x_f} 2xR(x)dx \\
Y_{Drr} &= -Z_{Dqq} &&= -\frac{1}{2}\rho c_{dc}\int_{x_t}^{x_f} 2x|x|R(x)dx \\
M_{Dqq} &= N_{Drr} &&= -\frac{1}{2}\rho c_{dc}\int_{x_t}^{x_f} 2x^2|x|R(x)dx \\
K_{Dpp} &= 0
\end{aligned} \tag{3.38}$$

where $R(x)$ is the radius along body-fixed axial direction, x_f is the axial forward position in the body-fixed frame, x_t is the axial tail position in the body-fixed frame, c_{dc} is the drag coefficient

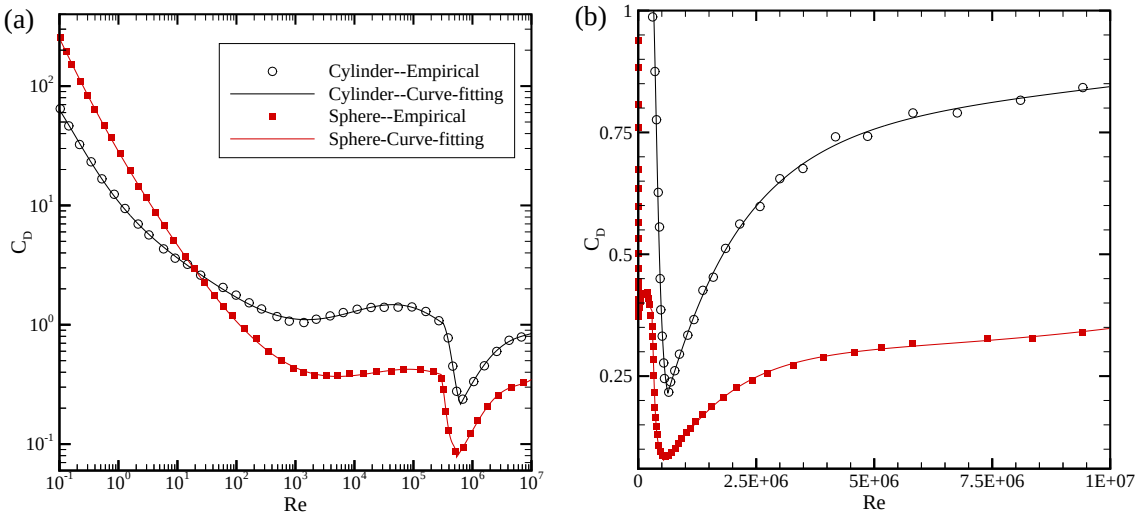

Figure 3.1. Drag coefficients as a function of Reynolds number for a smooth cylinder and sphere: (a) plotted in log scale; (b) plotted in linear scale

of a cylinder which is equal to 1.1 according to the approximation by Hoerner (1965). In current study, the rigid body is a cylinder, so $R(x) = d/2$.

Note that Equation (3.38) is based on the assumption that Reynolds number is larger than 10^5 and the flow is turbulent. For Re $<<$ 1, i.e., creeping or Stokes flows, the flow field can be solved analytically (Batchelor 1967), and the correspond drag coefficient can be expressed as

$$C_D = \frac{8\pi}{\mathrm{Re}\,\ln(7.4/\mathrm{Re})}. \tag{3.39}$$

To bridge the drag coefficients in different regimes, a general formula is developed based on Equation (3.38) for high Reynolds numbers, the empirical drag coefficient data for moderate Reynolds numbers (Munson et al. 1999), and the theoretical analysis for low Reynolds numbers (Equation [3.39]). Figure 3.1 shows the comparison of the simulated drag coefficients obtained via the general formula to the empirical drag coefficient data.

3.4.3 Total Drag Forces and Moments

By combining the axial and cross-flow drag coefficients, we can express the hydrodynamic drag forces and moments as

$$\begin{pmatrix} \mathbf{F_D} \\ \mathbf{M_D} \end{pmatrix} = \begin{pmatrix} X_D \\ Y_D \\ Z_D \\ K_D \\ M_D \\ N_D \end{pmatrix} = \begin{pmatrix} X_{Duu}(u-V_1)|u-V_1| \\ Y_{Dvv}(v-V_2)|v-V_2| + Y_{Drr}(r-\omega_3)|r-\omega_3| \\ Z_{Dww}(w-V_3)|w-V_3| + Z_{Dqq}(q-\omega_2)|q-\omega_2| \\ K_{Dpp}(p-\omega_1)|p-\omega_1| \\ M_{Dww}(w-V_3)|w-V_3| + M_{Dqq}(q-\omega_2)|q-\omega_2| \\ N_{Dvv}(v-V_2)|v-V_2| + N_{Drr}(r-\omega_3)|r-\omega_3| \end{pmatrix} \tag{3.40}$$

3.5 Lift Forces and Moments

When a rigid body immersed in a fluid moves, an interaction between the fluid and the body occurs, and the body experiences a resultant force. The component normal to the upstream velocity is termed the "lift." Theoretically, it can be expressed in terms of "pressure" and "shear stresses" and obtained by integrating pressure and shear-stress distributions on the surface of the body. However, it is usually extremely difficult to evaluate pressure and shear-stress distributions, especially shear-stress distribution. In cases where the contribution from the shear stress is relatively small compared with that from pressure, i.e., the resultant force mainly depends on pressure distribution, lift can be obtained experimentally by measuring pressure distribution along the body surface directly. For this investigation, before reliable experimental measurements are available, an empirical method is applied.

From Hoerner (1985), define Hoerner lift slope coefficient

$$c_{yd\beta} = c_{y\beta}\left(\frac{L}{d}\right)\left(\frac{180}{\pi}\right) \tag{3.41}$$

where coefficient $c_{y\beta}$ is determined empirically by the ratio of the length over diameter, L/d.

The corresponding lift coefficients are

$$Y_{Luv} = Z_{Luw} = -\frac{1}{2}\rho d^2 c_{yd\beta} \tag{3.42}$$

and the resultant lift forces are

$$\begin{aligned} Y_L &= Y_{Luv} uv \\ Z_L &= Z_{Luw} uw \end{aligned} \tag{3.43}$$

For lift moments, Hoerner (1965) found that the location of the resultant force is between 0.6 and 0.7 of the body length away from the forward position. Define

$$x_{cp} = -0.65L - x_f \tag{3.44}$$

where x_{cp} is the point of the resultant force, and the related lift moment coefficients and moments are

$$M_{Luw} = -N_{Luv} = Y_{Luv} x_{cp} = -\frac{1}{2}\rho d^2 c_{yd\beta} x_{cp} \tag{3.45}$$

$$\begin{aligned} M_L &= M_{Luw} uw \\ N_L &= N_{Luv} uv \end{aligned} \tag{3.46}$$

Include the flow field and rewrite the lift forces and moments in matrix form,

$$\begin{pmatrix} \mathbf{F_L} \\ \mathbf{M_L} \end{pmatrix} = \begin{pmatrix} X_L \\ Y_L \\ Z_L \\ K_L \\ M_L \\ N_L \end{pmatrix} = \begin{pmatrix} 0 \\ Y_{Luv}(u-V_1)(v-V_2) \\ Z_{Luw}(u-V_1)(w-V_3) \\ 0 \\ M_{Luw}(u-V_1)(w-V_3) \\ N_{Luv}(u-V_1)(v-V_2) \end{pmatrix} \tag{3.47}$$

3.6 Resultant Forces and Moments

Substitute the final expressions for hydrostatics (Equation [3.19]), drag (Equation [3.40]), added mass (Equation [3.33]), and lift (Equation [3.47]) into Equation (3.2), and normalize it with the object mass, then get

$$\begin{pmatrix} \sum F'_X \\ \sum F'_Y \\ \sum F'_Z \\ \sum M'_X \\ \sum M'_Y \\ \sum M'_Z \end{pmatrix} = \begin{pmatrix} \sum F_X/m \\ \sum F_Y/m \\ \sum F_Z/m \\ \sum M_X/m \\ \sum M_Y/m \\ \sum M_Z/m \end{pmatrix} = \frac{1}{m} \begin{pmatrix} X_{HS}+X_D+X_L+X_A \\ Y_{HS}+Y_D+Y_L+Y_A \\ Z_{HS}+Z_D+Z_L+Z_A \\ K_{HS}+K_D+K_L+K_A \\ M_{HS}+M_D+M_L+M_A \\ N_{HS}+N_D+N_L+N_A \end{pmatrix} \tag{3.48}$$

4.0 Simulation

This section provides simulation data and a test example describing five cases in which 6DOF motion of Sensor Fish are simulated for condition and flow.

4.1 Complete Equations of 6DOF Motion

Combine the equations for all the forces and moments, substitute them into the normalized equation of 6DOF motion for a rigid body (Equation [2.23]), and move acceleration terms of the added mass to the left side of the equations,

$$\begin{pmatrix} 1-X_{A\dot{u}}/m & 0 & 0 & 0 & z_g & -y_g \\ 0 & 1-Y_{A\dot{v}}/m & 0 & -z_g & 0 & x_g-Y_{A\dot{r}}/m \\ 0 & 0 & 1-Z_{A\dot{w}}/m & y_g & -x_g-Z_{A\dot{q}}/m & 0 \\ 0 & -z_g & y_g & I'_{xx}-K_{A\dot{p}}/m & -I'_{xy} & -I'_{xz} \\ z_g & 0 & -x_g-M_{A\dot{w}}/m & -I'_{xy} & I'_{yy}-M_{A\dot{q}}/m & -I'_{yz} \\ -y_g & x_g-N_{A\dot{v}}/m & 0 & -I'_{xz} & -I'_{yz} & I'_{zz}-N_{A\dot{r}}/m \end{pmatrix} \begin{pmatrix} \dot{u} \\ \dot{v} \\ \dot{w} \\ \dot{p} \\ \dot{q} \\ \dot{r} \end{pmatrix} =$$

$$\frac{1}{m}\begin{pmatrix} X_{HS}+X_D+X_L+X_A-X_{A\dot{u}}\dot{u} \\ Y_{HS}+Y_D+Y_L+Y_A-Y_{A\dot{v}}\dot{v}-Y_{A\dot{r}}\dot{r} \\ Z_{HS}+Z_D+Z_L+Z_A-Z_{A\dot{w}}\dot{w}-Z_{A\dot{q}}\dot{q} \\ K_{HS}+K_D+K_L+K_A-K_{A\dot{p}}\dot{p} \\ M_{HS}+M_D+M_L+M_A-M_{A\dot{q}}\dot{q}-M_{A\dot{w}}\dot{w} \\ N_{HS}+N_D+N_L+N_A-N_{A\dot{r}}\dot{r}-N_{A\dot{v}}\dot{v} \end{pmatrix} - \begin{pmatrix} f_1 \\ f_2 \\ f_3 \\ T_1 \\ T_2 \\ T_3 \end{pmatrix} = \begin{pmatrix} \sum F'_x - X_{A\dot{u}}\dot{u}/m - f_1 \\ \sum F'_y - (Y_{A\dot{v}}\dot{v}+Y_{A\dot{r}}\dot{r})/m - f_2 \\ \sum F'_z - (Z_{A\dot{w}}\dot{w}+Z_{A\dot{q}}\dot{q})/m - f_3 \\ \sum M'_x - K_{A\dot{p}}\dot{p}/m - T_1 \\ \sum M'_y - (M_{A\dot{q}}\dot{q}+M_{A\dot{w}}\dot{w})/m - T_2 \\ \sum M'_z - (N_{A\dot{r}}\dot{r}+N_{A\dot{v}}\dot{v})/m - T_3 \end{pmatrix} \tag{4.1}$$

where

$$\begin{aligned} f_1 &= -vr+wq-x_g(q^2+r^2)+y_gpq+z_gpr \\ f_2 &= -wq+ur-y_g(p^2+r^2)+z_gqr+x_gpq \\ f_3 &= -uq+vp-z_g(p^2+q^2)+x_gpr+y_gqr \\ T_1 &= (I'_{zz}-I'_{yy})qr-I'_{xz}pq+I'_{yz}(r^2-q^2)+I'_{xy}pr+y_g(-uq+vp)-z_g(-wp+ur)) \\ T_2 &= (I'_{xx}-I'_{zz})pr-I'_{xy}qr+I'_{zx}(p^2-r^2)+I'_{yz}pq+z_g(-vr+wq)-x_g(-uq+vp)) \\ T_3 &= (I'_{yy}-I'_{xx})pq-I'_{yz}pr+I'_{xy}(q^2-p^2)+I'_{zx}rq+x_g(-wp+ur)-y_g(-vr+wq)) \end{aligned} \tag{4.2}$$

Define

$$\mathbf{C} = \begin{pmatrix} 1 - X_{A\dot{u}}/m & 0 & 0 & 0 & z_g & -y_g \\ 0 & 1 - Y_{A\dot{v}}/m & 0 & -z_g & 0 & x_g - Y_{A\dot{r}}/m \\ 0 & 0 & 1 - Z_{A\dot{w}}/m & y_g & -x_g - Z_{A\dot{q}}/m & 0 \\ 0 & -z_g & y_g & I'_{xx} - K_{A\dot{p}}/m & -I'_{xy} & -I'_{xz} \\ z_g & 0 & -x_g - M_{A\dot{w}}/m & -I'_{xy} & I'_{yy} - M_{A\dot{q}}/m & -I'_{yz} \\ -y_g & x_g - N_{A\dot{v}}/m & 0 & -I'_{xz} & -I'_{yz} & I'_{zz} - N_{A\dot{r}}/m \end{pmatrix} \tag{4.3}$$

and Equation (4.2) becomes

$$\mathbf{C} \begin{pmatrix} \dot{u} \\ \dot{v} \\ \dot{w} \\ \dot{p} \\ \dot{q} \\ \dot{r} \end{pmatrix} = \begin{pmatrix} \sum F'_x - X_{A\dot{u}}\dot{u}/m - f_1 \\ \sum F'_y - (Y_{A\dot{v}}\dot{v} + Y_{A\dot{r}}\dot{r})/m - f_2 \\ \sum F'_z - (Z_{A\dot{w}}\dot{w} + Z_{A\dot{q}}\dot{q})/m - f_3 \\ \sum M'_x - K_{A\dot{p}}\dot{p}/m - T_1 \\ \sum M'_y - (M_{A\dot{q}}\dot{q} + M_{A\dot{w}}\dot{w})/m - T_2 \\ \sum M'_z - (N_{A\dot{r}}\dot{r} + N_{A\dot{v}}\dot{v})/m - T_3 \end{pmatrix}. \tag{4.4}$$

Let $\mathbf{H} = \mathbf{C}^{-1}$ and include the properties of quaternion and transformation, then obtain the final equations for simulation in matrix form:

$$\begin{pmatrix} \dot{\varepsilon}_1 \\ \dot{\varepsilon}_2 \\ \dot{\varepsilon}_3 \\ \dot{\varepsilon}_4 \end{pmatrix} = \frac{1}{2} \begin{pmatrix} 0 & r & -q & p \\ -r & 0 & p & q \\ q & -p & 0 & r \\ -p & -q & -r & 0 \end{pmatrix} \begin{pmatrix} \varepsilon_1 \\ \varepsilon_2 \\ \varepsilon_3 \\ \varepsilon_4 \end{pmatrix} \tag{4.5}$$

$$\begin{pmatrix} \dot{u} \\ \dot{v} \\ \dot{w} \\ \dot{p} \\ \dot{q} \\ \dot{r} \end{pmatrix} = \mathbf{H} \begin{pmatrix} \sum F'_x - X_{A\dot{u}}\dot{u}/m - f_1 \\ \sum F'_y - (Y_{A\dot{v}}\dot{v} + Y_{A\dot{r}}\dot{r})/m - f_2 \\ \sum F'_z - (Z_{A\dot{w}}\dot{w} + Z_{A\dot{q}}\dot{q})/m - f_3 \\ \sum M'_x - K_{A\dot{p}}\dot{p}/m - T_1 \\ \sum M'_y - (M_{A\dot{q}}\dot{q} + M_{A\dot{w}}\dot{w})/m - T_2 \\ \sum M'_z - (N_{A\dot{r}}\dot{r} + N_{A\dot{v}}\dot{v})/m - T_3 \end{pmatrix} \tag{4.6}$$

$$\begin{pmatrix} \dot{x} \\ \dot{y} \\ \dot{z} \end{pmatrix} = \mathbf{Q}^T \begin{pmatrix} u \\ v \\ w \end{pmatrix}. \tag{4.7}$$

Note that in Equation (4.6) the acceleration terms on the right side of the equation are cancelled by the corresponding terms of the added mass (see Equation [3.33]), that is, all the acceleration terms appear only on the left side of the equation.

4.2 Numerical Simulation

The final equation of 6DOF motion is a set of 13 first-order nonlinear different equations. As noted earlier, the acceleration terms on the right side of the differential equations for the velocities are cancelled by the corresponding terms of the added mass, and all the forces and moments

coefficients are defined explicitly. Given initial values at $t = 0$,

$$\begin{array}{lll} x(0) = x_0 & y(0) = y_0 & z(0) = z_0 \\ \phi(0) = \phi_0 & \theta(0) = \theta_0 & \psi(0) = \psi_0 \\ u(0) = u_0 & v(0) = v_0 & w(0) = w_0 \\ p(0) = p_0 & q(0) = q_0 & r(0) = r_0 \end{array} \tag{4.8}$$

initial values for the quaternion components $\varepsilon(0) = (\varepsilon_1(0), \varepsilon_2(0), \varepsilon_3(0), \varepsilon_4(0))^T$ are obtained via Equations (2.1) and (2.10). Finally, the equation of motion is solved by an explicit Runge-Kutta (4,5) formula, the Dormand-Prince pair.

4.3 Test Examples

4.3.1 Terminal Settling Velocity of a Falling Sphere in a Viscous Fluid

The solver is validated by Stokes flow around a sphere. When a sphere reaches terminal velocity,

$$W - B + F_D = 0 \tag{4.9}$$

$$W - B = (\rho_o - \rho) g (\frac{\pi}{6} d^3) \tag{4.10}$$

$$F_D = \frac{1}{2} \rho U^2 A C_D = \frac{1}{2} \rho U^2 (\frac{\pi}{4} d^2) C_D \tag{4.11}$$

where W is the weight of sphere, B is buoyancy, F_D is drag, C_D is drag coefficient, ρ_o is the density of the sphere, ρ is the density of water, U is the terminal velocity, A is the reference area, and d is the diameter of the sphere.

For Stokes flow around a sphere, $\mathrm{Re} = \frac{UD\rho}{\mu} << 1$ and $C_D = \frac{24}{\mathrm{Re}}$, where μ is the dynamic viscosity of water,

$$F_D = 3\pi\mu U d \tag{4.12}$$

then

$$U = \frac{(\rho_o - \rho) g d^2}{18\mu} \tag{4.13}$$

Example: $d = 0.1$ mm, $\rho_o = 1600\ kg/m^3$, $\rho = 1000\ kg/m^3$, $\mu = 1.12 \times 10^{-3} N \cdot s/m^2$. From Equation (4.13), U is $2.917 \times 10^{-3}\ m/s$. For comparison, from simulation, the terminal velocity is also $2.917 \times 10^{-3}\ m/s$, as shown in Figure 4.1.

4.3.2 Motion of an Ellipsoid at Low Reynolds Numbers

Zhang et al. (2001) derived equations of motion for an ellipsoidal particle entrained by a turbulent flow velocity field. They used classical analytical expressions describing the forces and torques acting on the body for low Reynolds number, as determined by the magnitude of the relative velocity between the flow field and the body. For these dynamic equations of motion, the

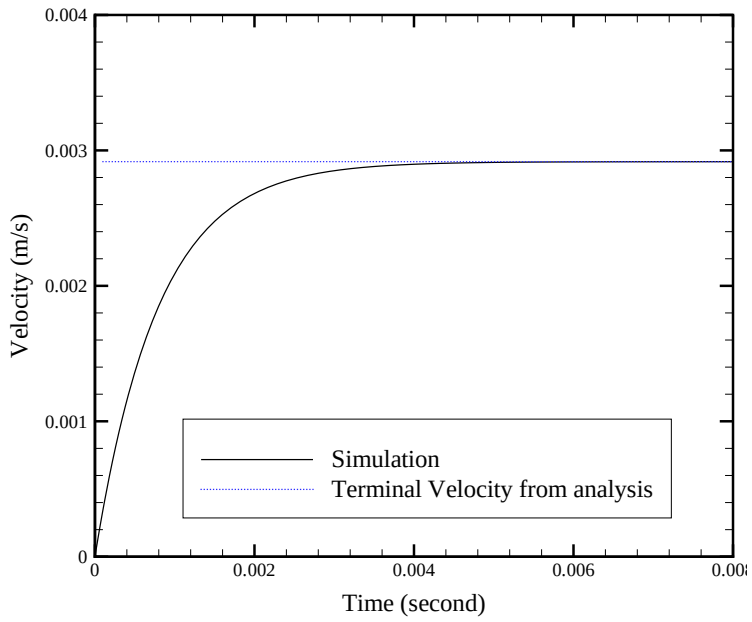

Figure 4.1. Terminal velocity of a sphere at Re $<<$ 1

slip velocity is assumed sufficiently small so the entrainment takes place in the so called "creeping flow regime." In particular, for this regime of flow, the hydrodynamic drag and shear-induced lift tend to be directly proportional (linearly) to the velocity difference between the flow and body motion.

In their investigation of ellipsoidal particles transport, Newton's second law was solved in the inertial frame, while Euler's motion equation of angular velocities was solved in the body-fixed frame. However, in our study, it was more convenient and efficient to write all the equations of motion in only the body-fixed frame. The details of derivation are included in Appendix A.

As a test example, a 5:1 ellipsoid, 5 *cm* long by 1 *cm* diameter, is simulated. The ellipsoid density ρ_o is taken as 1,200 kg/m^3 compared with 1,000 kg/m^3 for water, so that it sinks. The ellipsoid's geometric center coincides with the center of mass.

The parabolic velocity varies in the x direction, with the flow pointing negatively along the y-axis. Thus, shear gradient is along the x direction. A constant velocity component acts along the z-axis as well, pointing in the negative direction. The acceleration of gravity is applied along the y-axis for this example, in a positive direction in opposition to the parabolic velocity field, while gravity is usually applied in positive inertial z-direction elsewhere in this report. The velocity field is specifically given as

$$\begin{aligned} V_x &= 0 \\ V_y &= -\frac{20}{W_f}\, x\,(1-\frac{x}{W_f}) \qquad \text{for} \quad 0<x<W \\ V_z &= -1 \end{aligned} \tag{4.14}$$

where W_f is the width of the parabolic flow field and taken to be 1 and 10 m for two test cases.

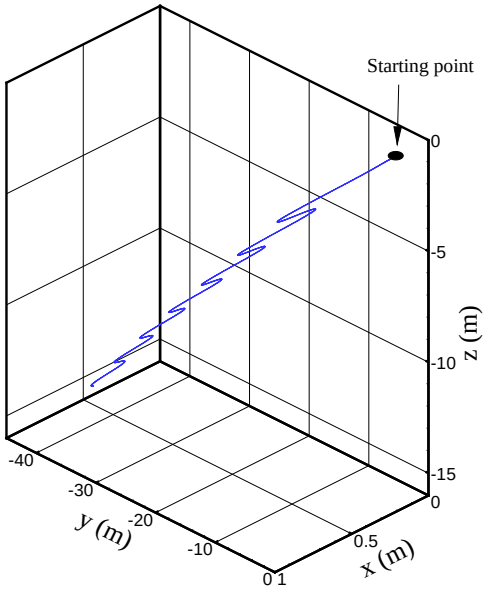

Figure 4.2. Trajectory of an ellipsoid in a 1-m-wide parabolic velocity field

A typical trajectory for the 1-m-wide velocity field is shown in Figure 4.2. The ellipsoid major axis is aligned with the flow initially, and turns very little during the simulation period of 15 seconds. During this period, drag force overcomes gravity, and the ellipsoid moves with the flow in the negative y-direction. The ellipsoid is started at $x = 0.25$ and oscillates back and forth across the velocity center line.

The motion is described in more detail by display of each component below (Figure 4.3). In this case, the ellipsoid has an initial angle of 45 degrees with the flow direction. Its rotation rate about its body-fixed Y-axis, which points parallel to the inertial z-axis is shown also, with the clockwise rotation being the positive direction. Its rotation indicates turning and then a reversal. The drag with flow in the negative y-direction overcomes the gravity in the opposite direction. Nevertheless, this still causes the velocity of the ellipsoid to be less than if fully entrained without gravity opposing. Note the ellipsoid initially turns inward toward the center of the flow, 45 degrees, is first turned outward passing over the centered direction. It continues past the center and returns again. Its direction appears to approach being parallel to the flow. Also, there is no turning out of the inertial x-y plane since the velocity component in the z-axis direction is uniform everywhere.

The case with velocity shear width of 10 m is plotted in Figure 4.4. The period is increased to 30 seconds to let the trajectory develop more. Clearly, the frequency of oscillation back and forth across the shear is reduced substantially. In this case, the vertical excursions against gravity have greater amplitude than for the 1 m shear. The pull of gravity is beginning to reverse the direction of movement in opposition to the flow drag. In fact, the ellipsoid path has reversed direction of travel.

In both cases, the rotation begins so that the ellipsoid turns outward from the flow field center. This reduces the initial angle and turns the ellipsoid initially back into alignment with the flow

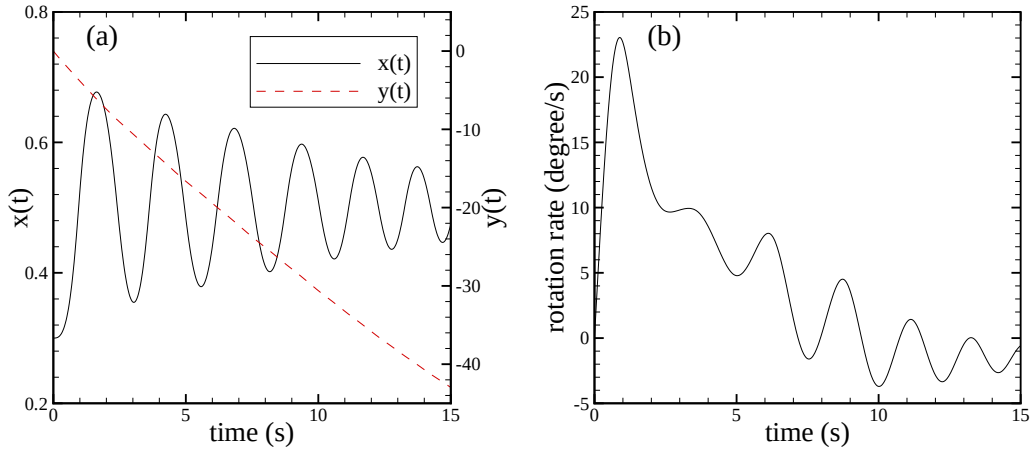

Figure 4.3. Ellipsoid Trajectory Components in 1-m-wide parabolic shear flow. Ellipsoid is initially turned 45 degrees to the flow direction, toward the flow center. Rotation is about the inertial Z-axis.

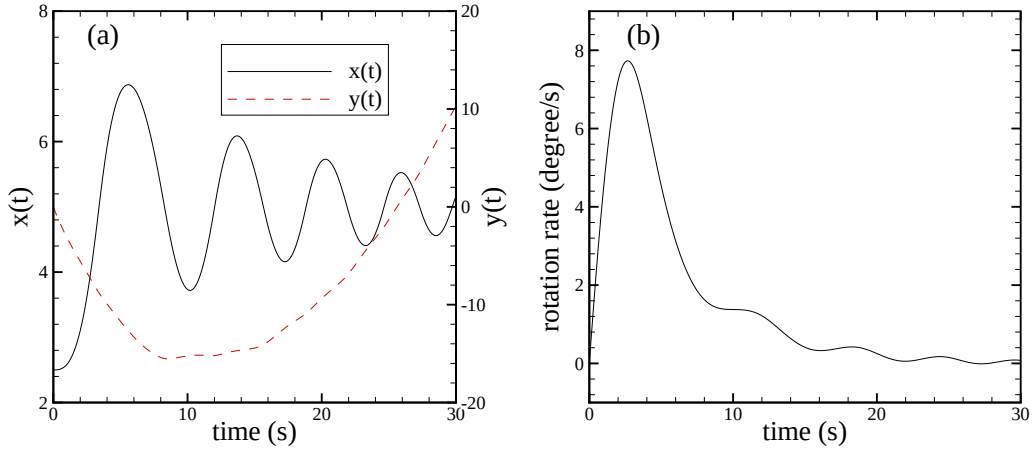

Figure 4.4. Ellipsoid Trajectory Components in 10-m-wide parabolic shear flow. Ellipsoid is initially turned 45 degrees into flow direction, toward the flow center. Rotation is about the inertial Z-axis.

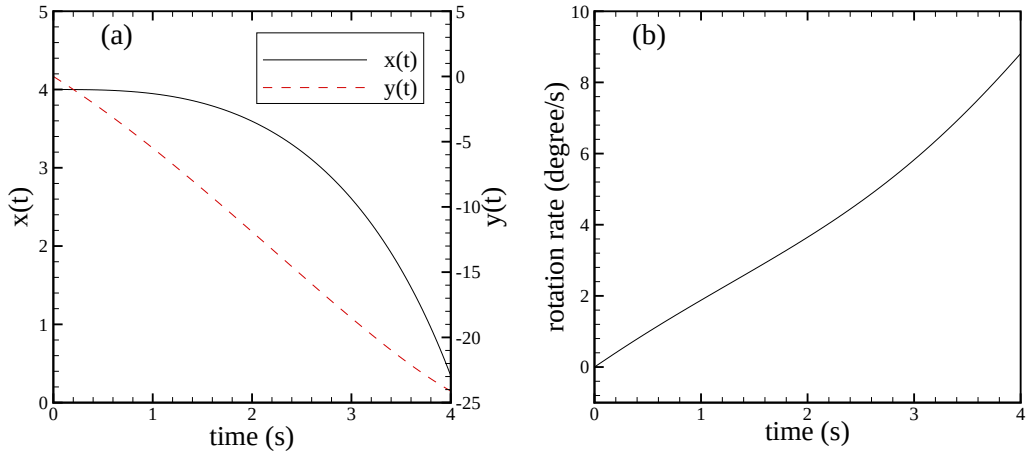

Figure 4.5. Ellipsoid Trajectory Components in 10-m-wide parabolic shear flow. Ellipsoid is initially turned 45 degrees into flow direction, toward the flow center. Rotation is about the inertial Z-axis. With the direction of gravity points in the same direction of flow.

direction. It overshoots alignment, and then turns back again.

It is noteworthy that when the ellipsoid starts at the center of the shear field, it does not oscillate across. Then, ideally, it remains at the center as it eventually travels in the positive y-direction, sinking down with gravity against the flow.

If instead, the direction of gravity points in the same direction of flow, negative y-direction, then the ellipsoid will not oscillate about the center line, but progresses toward the nearest boundary. For instance, as shown in Figure 4.5, if started at $x = 4$ m for the 10-m-wide parabolic field, it will reach $x = 0$ in about 4 seconds. Starting with a 45 degree tilt as before, it turns back outward by about 16 degrees in this period.

These figures and predicted behavior in a parabolic velocity field tend to correspond to the similar trajectory behavior reported by Saffman (1965) and Feng and Josepth (1995). Similar complex motions have also been discussed by Broday et al. (1998). An issue, however, is whether the examples given here apply a velocity magnitude that causes the shear-lift formula to go outside the accepted range of Reynolds number. In any case, the predicted ellipsoid motion is at least representative.

4.3.3 Six Degree of Freedom Motion of Sensor Fish

Six degree of freedom motion of Sensor Fish were simulated for seven sets of initial conditions and ambient flows, which are defined as cases 1 to 7. Note that the forces and moments are high-Reynolds number approximations based on available information. Additional experimental and computational work is planned to develop relationships that are specific to the Sensor Fish body and range of Reynolds numbers it experiences during field deployment.

Test cases 1 through 5 are in uniform flows and have the same initial conditions:

$$\begin{array}{ccc} x(0)=0 & y(0)=0 & z(0)=0 \\ \phi(0)=40^\circ & \theta(0)=30^\circ & \psi(0)=20^\circ \\ u(0)=0 & v(0)=0 & w(0)=0 \\ p(0)=0 & q(0)=0 & r(0)=0. \end{array} \tag{4.15}$$

Cases 6 and 7 are in parabolic flow field, and the initial position has been changed to

$$x(0)=0 \quad y(0)=1\,m \quad z(0)=0. \tag{4.16}$$

For all the seven cases, the corresponding initial quaternion values are

$$\varepsilon_1(0)=0.2831 \quad \varepsilon_2(0)=0.2969 \quad \varepsilon_3(0)=0.07044 \quad \varepsilon_4(0)=0.9093 \tag{4.17}$$

In addition, suppose $L=10$ *cm*, $d=2$ *cm*, and Sensor Fish is neutrally buoyant. Other parameters and animation movie files are listed in Table 4.1. The movie files are included in the attached CD.

	$(x_g,y_g,z_g),cm$	$V_x,m/s$	$V_y,m/s$	$V_z,m/s$	Animation filename
Case 1	$(2,0,0)$	0	0	0	Case1.avi
Case 2	$(2,0,0)$	2	0	0	Case2.avi
Case 3	$(0,0,0)$	2	0	0	Case3.avi
Case 4	$(2,0,0)$	2	1	0	Case4.avi
Case 5	$(0,0,0)$	2	1	0	Case5.avi
Case 6	$(2,0,0)$	$4-y^2$	0	0.5	Case6.avi
Case 7	$(0,0,0)$	$4-y^2$	0	0.5	Case7.avi

Table 4.1. Simulation Parameters and animation movie files for the seven test cases

For case 1, there is no ambient flow, but due to initial angles and the offset of center of mass from the geometric center, the resultant moment leads to the rotation of Sensor Fish. As shown in Figure 4.6, the rotation will die down due to the work of resistant drag, and there is slight motion on the z-direction due to the transition of rotational energy to translation energy. A snapshot of 6DOF motion of Sensor Fish is shown in Figure 4.7.

For cases 2 and 3, the ambient flow is an one-dimensional uniform flow field. As illustrated in Figures 4.8 and 4.9, an offset of center of mass (case 2) increases rotation of Sensor Fish in the first two seconds. A side-by-side comparison animation movie (Case2-3_side.avi) is included in the enclosed animation CD.

When the ambient flow field changes to a two-dimensional uniform flow, as in cases 4 and 5 shown in Figures 4.10 and 4.11, and the side-by-side comparison movie (Case4-5_side.avi), the Sensor Fish displays similar behavior as in cases 2 and 3; an offset of the center of mass leads to an increase in Sensor Fish rotation.

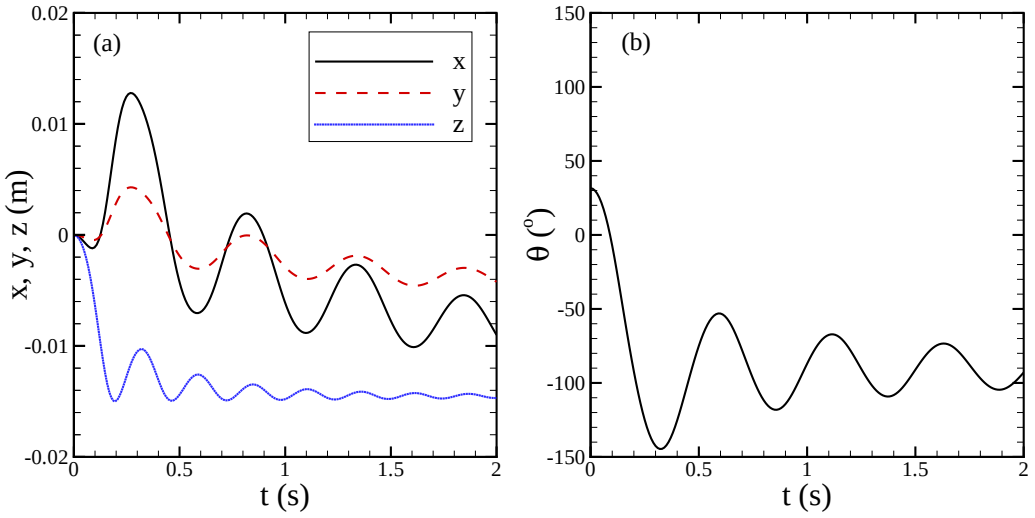

Figure 4.6. Trajectory of Sensor Fish for case 1, (a) x(t), y(t), and z(t); (b) $\theta(t)$

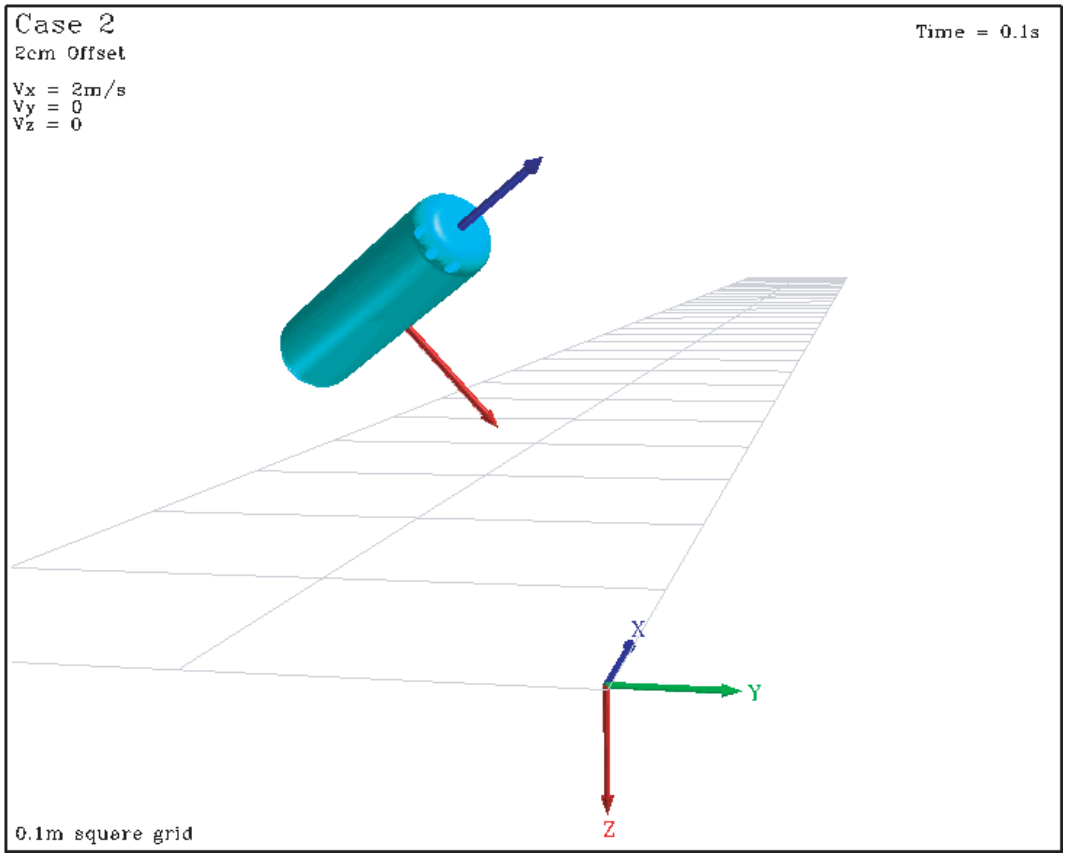

Figure 4.7. A snapshot of 6DOF motion of Sensor Fish

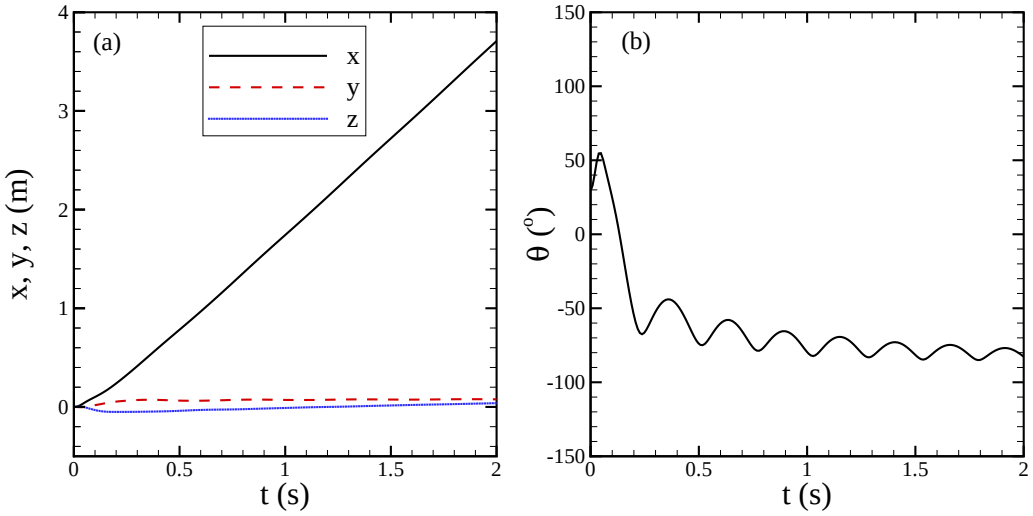

Figure 4.8. Trajectory of Sensor Fish for case 2 in one-dimensional uniform flow with an offset between mass center and geometric center of Sensor Fish, (a) x(t), y(t), and z(t); (b) $\theta(t)$

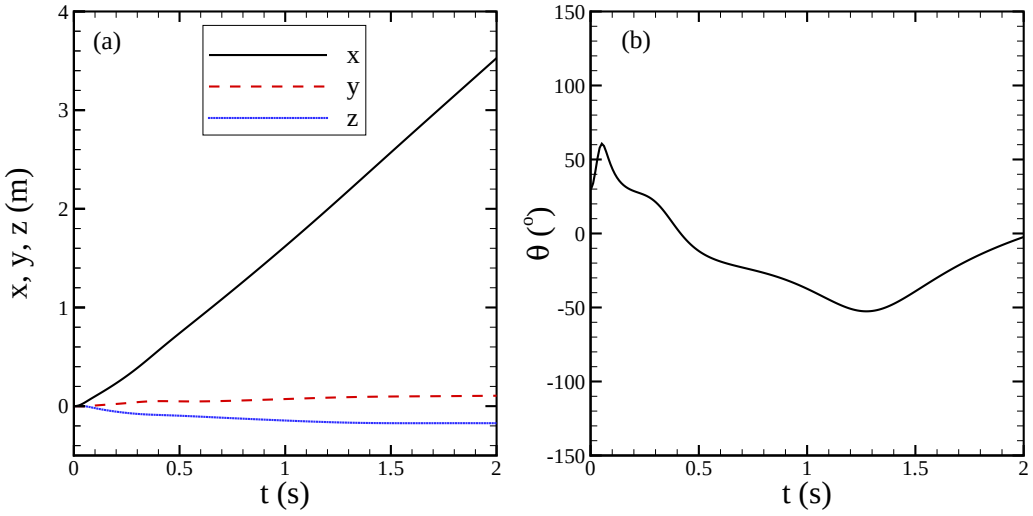

Figure 4.9. Trajectory of Sensor Fish for case 3 in one-dimensional uniform flow with mass center and geometric center of Sensor Fish overlapped, (a) x(t), y(t), and z(t); (b) $\theta(t)$

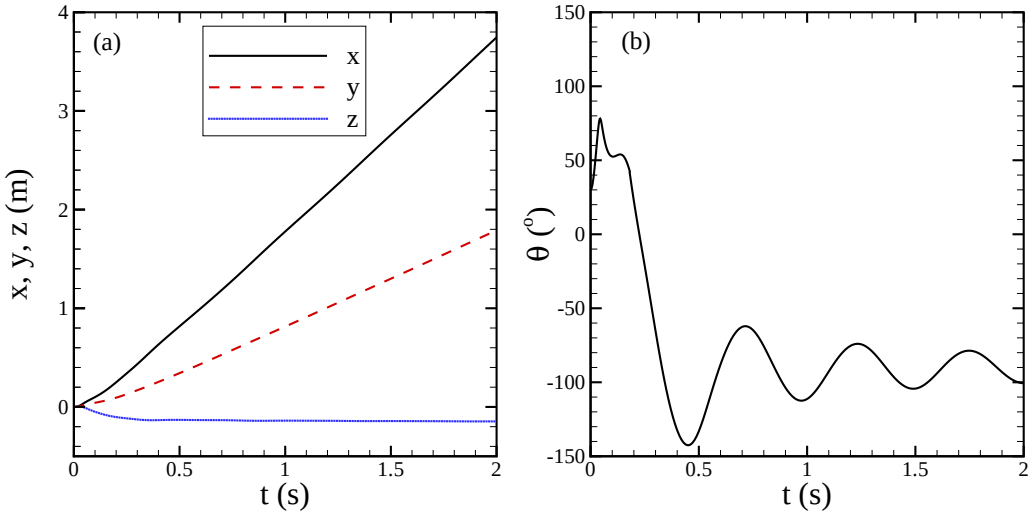

Figure 4.10. Trajectory of Sensor Fish for case 4 in two-dimensional uniform flow with an offset between mass center and geometric center of Sensor Fish, (a) x(t), y(t), and z(t); (b) $\theta(t)$

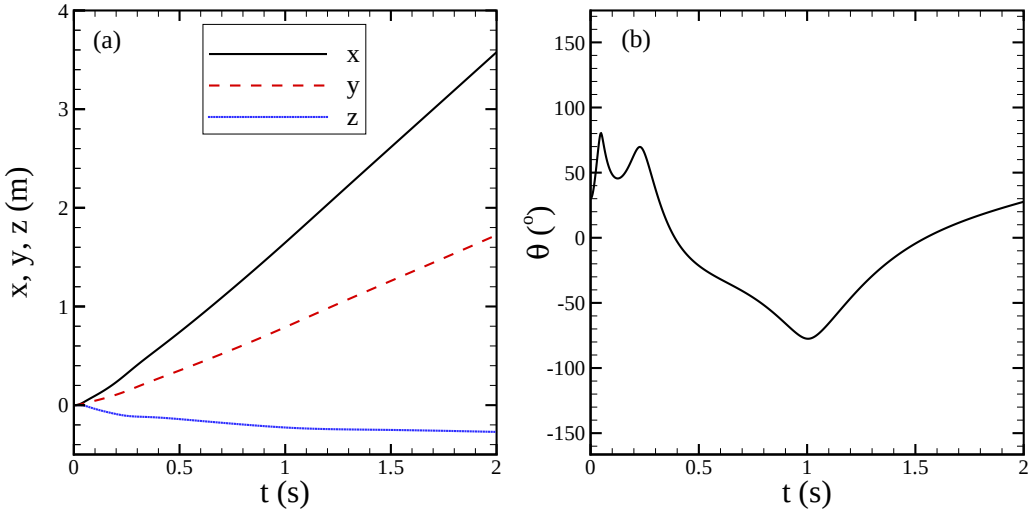

Figure 4.11. Trajectory of Sensor Fish for case 5 in two-dimensional uniform flow with mass center and geometric center of Sensor Fish overlapped, (a) x(t), y(t), and z(t); (b) $\theta(t)$

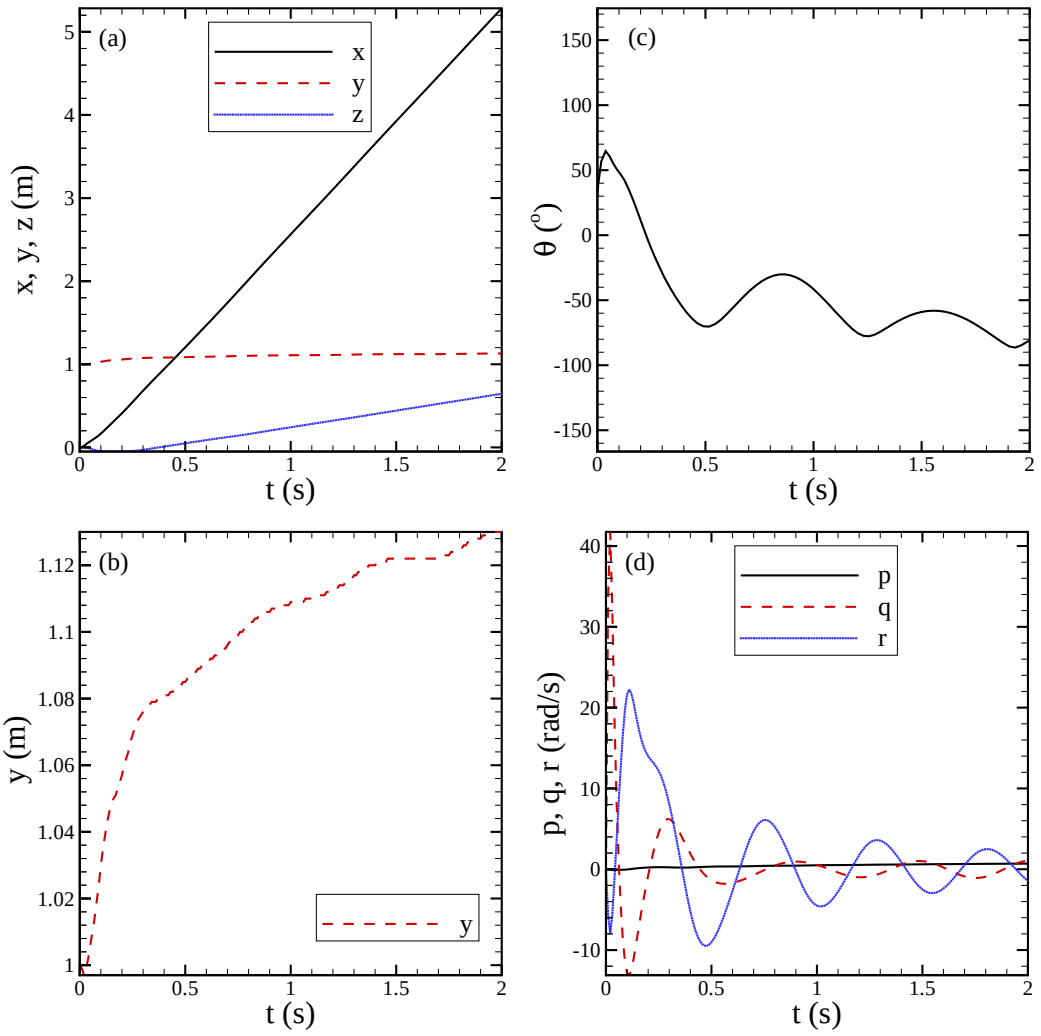

Figure 4.12. Trajectory and angular velocity of Sensor Fish for case 6 in parabolic flow field with an offset between mass center and geometric center of Sensor Fish, (a) x(t), y(t), and z(t); (b) y(t); (c) $\theta(t)$; (d) p(t), q(t), r(t)

For Sensor Fish in a parabolic flow field as in cases 6 and 7, besides the oscillating effect of deviation of the mass center as shown in Figures 4.12(c)(d) and 4.13(c)(d), there is a drift in y-direction (Figures 4.12b and 4.13b) due to the shear effect in that direction. A comparison movie (Case6-7_side.avi) for these two cases is also included in the CD.

However, it is important to point out that for all the examples tested, the oscillation effect due to the offset between the geometric center and mass center generally tends to diminish, and the Sensor Fish begins to align to the flow direction after several seconds, while the low-frequency oscillation of the cases without the offset continues to exist.

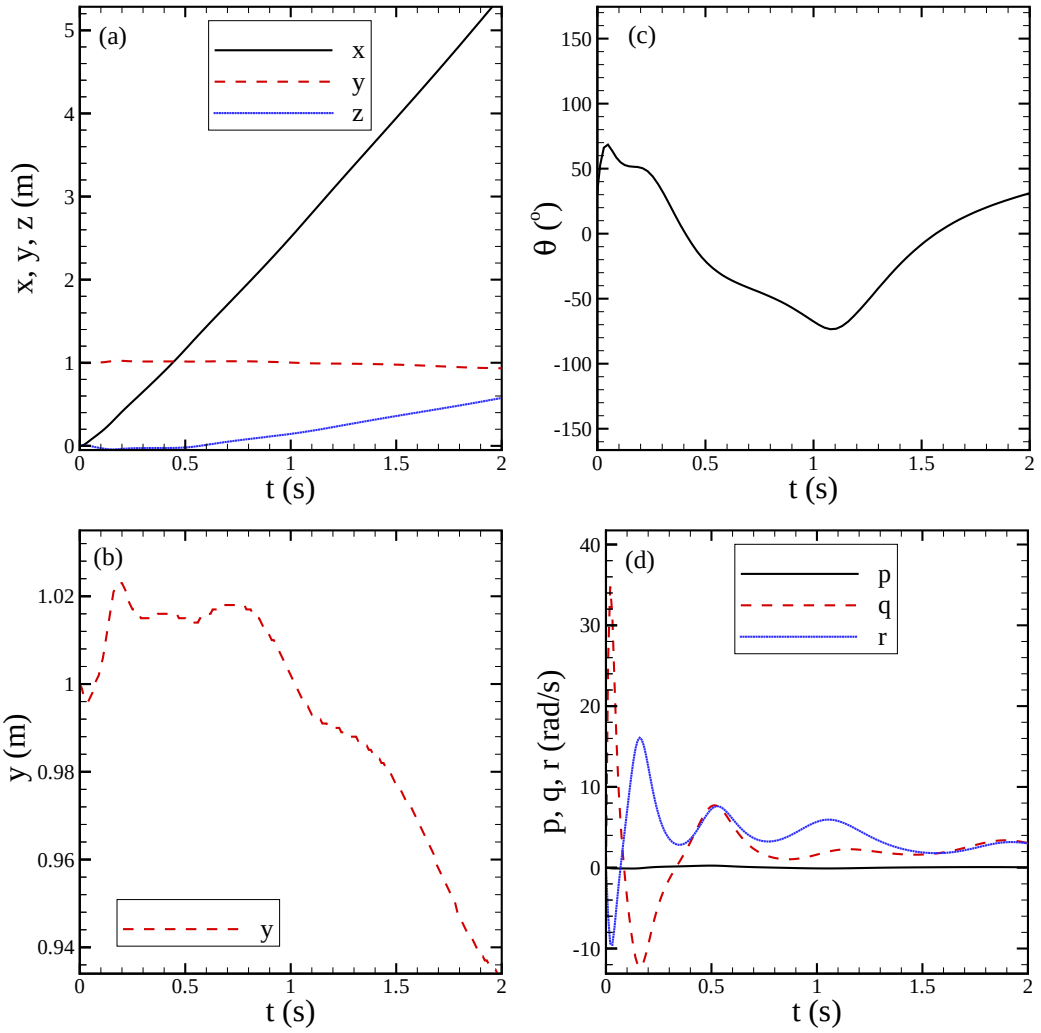

Figure 4.13. Trajectory and angular velocity of Sensor Fish for case 7 in parabolic flow field with mass center and geometric center of Sensor Fish overlapped, (a) x(t), y(t), and z(t); (b) y(t); (c) $\theta(t)$; (d) p(t), q(t), r(t)

5.0 Summary

As part of the process of redesigning the current 3DOF Sensor Fish device rate gyros will be added to the new six degree of freedom (6DOF) device to measure each of the six linear and angular accelerations. However, before the 6DOF Sensor Fish device can be developed and deployed, governing equations of motion must be developed in order to understand the design implications of instrument selection and placement within the body of the device.

As part of the initial steps in the design process, this report developed a fairly general formulation for the coordinate systems, equations of motion, force and moment relationships necessary to simulate the the 6DOF movement of an underwater body. Some simplifications are made by considering the Sensor Fish device to be a rigid, axisymmetric body. The equations of motion are written in the body-fixed frame of reference. Transformations between the body-fixed and inertial reference frames are performed using a formulation based on quaternions. Force and moment relationships specific to the Sensor Fish body are currently not available. However, examples of the trajectory simulations using the 6DOF equations are presented using existing low and high-Reynolds number force and moment correlations. Animation files for the test cases are provided in an attached CD.

The next phase of the work will focus on the refinement and application of the 6DOF simulator developed in this project. Experimental and computational studies are planned to develop a set of force and moment relationships that are specific to the Sensor Fish body over the range of Reynolds numbers that it experiences. Lab testing of prototype 6DOF Sensor Fish will also allow for refinement of the trajectory simulations through comparison with observations in test flumes. The 6DOF simulator will also be an essential component in tools to analyze field data measured using the next generation Sensor Fish. The 6DOF simulator will be embedded in a moving-machinery computational fluid dynamics (CFD) model for hydroturbines to numerically simulate the 6DOF Sensor Fish.

6.0 References

Batchelor GK. 1967. *An Introduction to Fluid Dynamics*. Cambridge University Press, Cambridge, United Kingdom.

Becker JM, CS Abernethy, and DD Dauble. 2003. "Identifying the Effects on Fish of Changes in Water Pressure During Turbine Passage." *Hydro Review* 5:32–42.

Blevins RD. 1993. *Formulas for Natural Frequency and Mode Shape*. Krieger Publishing Company, Melbourne, Florida.

Broday D, M Fichman, M Shapiro, and C Gutfinger. 1998. "Motion of Spheroidal Particles in Vertical Shear Flows." *Physics of Fluids* 10:86–100.

Carlson TJ. 2001. *Proceedings of the Turbine Passage Survival Workshop, Portland, Oregon*. PNNL-SA-33996, Pacific Northwest National Laboratory, Richland, Washington.

Carlson TJ and JP Duncan. 2003. *Evolution of the Sensor Fish Device for Measuring Physical Conditions in Severe Hydraulic Environments*. DOE/ID-11079, U.S. Department of Energy Idaho Operations Office, Idaho Falls, Idaho.

Carlson TJ, JP Duncan, and TL Gilbride. 2003. "The Sensor Fish: Measuring Fish Passage in Severe Hydraulic Conditions." *Hydro Review* XXII:62–69.

Čada GF. 1998. "Better Science Supports Fish-Friendly Turbine Designs." *Hydro Review* XVII:52–61.

Čada GF. 2001. "The Development of Advanced Hydroelectirc Turbines to Improve Fish Passage Survival." *Fishery* 26:14–23.

Conte G and A Serrani. 1996. "Modelling and Simulation of Underwater Vehicles." In *Proceedings of the 1996 IEEE International Symmposium on Computer-Aided Control System Design*, pp. 61–67. IEEE, Dearborn, Michigan.

Feng J and DD Josepth. 1995. "The Unsteady Motion of Solid Bodies in Creeping Flow." *Journal of Fluid Mechanics* 303:83–102.

Fossen TI. 1994. *Guidance and Control of Ocean Vehicles*. John Wiley & Sons, New York.

Happel J and H Brenner. 1983. *Low Reynolds Number Hydrodynamics*. Kluwer, Boston.

Harper EY and ID Chang. 1968. "Maximum Dissipation Resulting from Lift in a Slow Viscous Shear Flow." *Journal of Fluid Mechanics* 33:209–225.

Hoerner SF. 1965. *Fluid Dynamics Drag*. Hoerner Fluid Dynamics, Brick Town, New Jersey.

Hoerner SF. 1985. *Fluid Dynamics Lift*. Hoerner Fluid Dynamics, Brick Town, New Jersey.

Hughes PC. 1986. *Spacecraft Attitude Dynamics*. John Wiley & Sons, New York.

Jeffery GB. 1922. "The Motion of Ellipsoid Particles Immersed in a Viscous Fluid." *Proceedings of Royal Society* 102:161–179.

Maxey MR and JJ Riley. 1983. "Equation of Motion for a Small Rigid Sphere in a Nonuniform Flow." *Physics of Fluids* 26:883–889.

Mougin G and J Magnaudet. 2002. "The Generalized Kirchhoff Equations and their Application to the Interaction Between a Rigid Body and an Arbitrary Time-Dependent Viscous Flow." *International Journal of Multiphase Flow* 28:1837–1851.

Munson BR, DF Young, and TH Okiishi. 1999. *Fundamentals of Fluid Mechanics*. John Wiley & Sons, New York.

Newman JN. 1977. *Marine Hydrodynamics*. MIT Press, Cambridge, Massachusetts.

Nietzel DA, MC Richmond, DD Dauble, RP Mueller, RA Moursund, CS Abernethy, GR Guensch, and GF Ćada. 2000. *Laboratory Studies on the Effects of Shear on Fish: Final Report*. DOE/ID-10822, U.S. Department of Energy Idaho Operations Office, Idaho Falls, Idaho.

Prestero T. 2001. "Verification of a Six-Degree of Freedom Simulation Model for the REMUS Autonomous Underwater Vehicle." Master's thesis, Massachusetts Institute of Technology, Cambridge, Massachusetts.

Richmond MC, TJ Carlson, JA Serkowski, CB Cook, and JP Duncan. 2004. "Characterizing the Fish-Passage Environment at The Dalles Dam Spillway." In *2004 World Water and Environmental Resouces Congress*. Salt Lake City, Utah.

Saffman PG. 1965. "The Lift on a Small Sphere in a Slow Shear Flow." *Journal of Fluid Mechanics* 22:385–400.

Shi L, JM Doster, and CW Mayo. 1999. "Drag Coefficient for Reactor Loose Parts." *Nuclear Technology* 127:24–37.

Wertz JR. 1985. *Spacecraft Attitude Determination and Control*. D. Reidel Publishing Company, Boston.

Zhang H, G Ahmadi, F Fan, and JB McLaughlin. 2001. "Ellipsoidal Particles Transport and Deposition in Turbulent Channel Flows." *International Journal of Multiphase Flow* 27:971–1009.

Appendix A

Ellipsoid Motion Equations for Low Reynolds Numbers

Appendix A: Ellipsoid Motion Equations for Low Reynolds Numbers

Zhang et al. (2001) derived equations of motion for an ellipsoidal particle entrained in turbulent channel flows. The slip velocity is assumed sufficiently small so that the forces and torques (moments) acting on the body are obtained from the expressions for the low-Reynolds number or creeping flow regime. In this flow regime, the hydrodynamic drag and shear-induced lift tend to be directly proportional (linearly) to the slip velocity. They wrote the translational equations of motion, i.e., Newton's law of $F = ma$, in the inertial reference frame. However, the equations for rotational motion were given in terms of the body-fixed frame with angular velocity components around this frame.

In the formulation of the motion equations presented in this report, all the forces and moments are expressed in the body-fixed frame. To be consistent, we adapt the formulation of Zhang et al. (2001) accordingly. In addition, in this Appendix, the semi-major axis is Z-axis instead of X-axis as in the main report.

Recall that the flow field has (V_x, V_y, V_z) in the inertial frame and (V_1, V_2, V_3) in the body-fixed frame as discussed in Chapter 3.1 (Page 11), then in the body-fixed frame, the drag force becomes

$$\mathbf{F_D} = \mu\pi a\mathbf{K}\cdot\begin{pmatrix} V_1-u \\ V_2-v \\ V_3-w \end{pmatrix} \tag{A.1}$$

where a is the semi-minor axis of the ellipsoid of revolution and

$$\mathbf{K} = \begin{pmatrix} k_x & 0 & 0 \\ 0 & k_y & 0 \\ 0 & 0 & k_z \end{pmatrix} \tag{A.2}$$

is called the translation dyadic. For the ellipsoid rotated around the Z-axis, it is determined by $\beta = b/a$ (ratio of semi-major axis to semi-minor axis)

$$k_x = k_y = \frac{16(\beta^2-1)}{(2\beta^2-3)\frac{\ln(\beta+\sqrt{(\beta^2-1)})}{\sqrt{(\beta^2-1)}}+\beta} \tag{A.3}$$

$$k_z = \frac{8(\beta^2-1)}{(2\beta^2-1)\frac{\ln(\beta+\sqrt{(\beta^2-1)})}{\sqrt{(\beta^2-1)}}-\beta} \tag{A.4}$$

Note that the semi-major axis is aligned along the body-fixed Z-axis and

$$\mathbf{Q}^{-1}\cdot\mathbf{K}\cdot\mathbf{Q}$$

is the dyadic in the inertial frame.

The shear-induced lift force for an arbitrary-shaped particle was obtained by Harper and Chang (1968) and the equation for it was re-stated by Zhang et al. (2001).

In the body-fixed frame, the lift force is

$$\mathbf{F_L} = \frac{\mu\pi^2 a^2}{\sqrt{\nu}} \cdot \sqrt{\left|\frac{\partial V_x}{\partial y}\right|} \cdot \mathbf{S'_x} \cdot (\mathbf{K} \cdot \mathbf{D'_x} \cdot \mathbf{K}) \cdot \begin{pmatrix} V_1 - u \\ V_2 - v \\ V_3 - w \end{pmatrix} \tag{A.5}$$

where

$$\mathbf{D'_x} = \mathbf{Q} \cdot \mathbf{D_x} \cdot \mathbf{Q}^{-1} \tag{A.6}$$

with

$$\mathbf{D_x} = \begin{pmatrix} 0.0501 & 0.0329 & 0 \\ 0.0182 & 0.0173 & 0 \\ 0 & 0 & 0.0373 \end{pmatrix} \tag{A.7}$$

being a special matrix that remains fixed, and

$$\mathbf{S'_x} = \mathbf{Q} \cdot \mathbf{S_x} \cdot \mathbf{Q}^{-1} \tag{A.8}$$

with

$$\mathbf{S_x} = \begin{pmatrix} 1 & 0 & 0 \\ 0 & \text{sign}\left(\frac{\partial V_x}{\partial y}\right) & 0 \\ 0 & 0 & 1 \end{pmatrix} \tag{A.9}$$

This force applies only for a flow field in the x-direction with shear in only the orthogonal y-direction. For flow in the y-direction as well, with shear in the x-direction, a similar additional force would likely need to be superimposed. Then arrangement of elements in $\mathbf{S_x}$ would need to be changed to describe the orthogonal shear direction.

In particular, to find shear-lift in the orthogonal direction replace $\mathbf{D_x}$ by $\mathbf{D_y}$ given below and replace the x-component flow velocity gradient with respect to y by the y-component velocity gradient with respect to x

$$\mathbf{D'_y} = \mathbf{Q} \cdot \mathbf{D_y} \cdot \mathbf{Q}^{-1} \tag{A.10}$$

and

$$\mathbf{D_y} = \begin{pmatrix} 0.0173 & 0.0182 & 0 \\ 0.0329 & 0.0501 & 0 \\ 0 & 0 & 0.0373 \end{pmatrix} \tag{A.11}$$

Thus the orthogonal lift is

$$\mathbf{F_L} = \frac{\mu\pi^2 a^2}{\sqrt{\nu}} \cdot \sqrt{\left|\frac{\partial V_y}{\partial x}\right|} \cdot \mathbf{S'_y} \cdot (\mathbf{K} \cdot \mathbf{D'_y} \cdot \mathbf{K}) \cdot \begin{pmatrix} V_1 - u \\ V_2 - v \\ V_3 - w \end{pmatrix} \tag{A.12}$$

where

$$\mathbf{S}'_{\mathbf{y}} = \mathbf{Q} \cdot \mathbf{S}_{\mathbf{y}} \cdot \mathbf{Q}^{-1} \tag{A.13}$$

and

$$\mathbf{S}_{\mathbf{y}} = \begin{pmatrix} \text{sign}\left(\frac{\partial V_y}{\partial x}\right) & 0 & 0 \\ 0 & 1 & 0 \\ 0 & 0 & 1 \end{pmatrix} \tag{A.14}$$

In general, the two force expressions for shear-lift are added together when flow is neither entirely in the x or y directions. In this trajectory model, shear in the vertical z-direction is presumed not to occur, or is presumed minor.

Zhang et al. (2001) pointed out that Jeffery (1922) originally derived the torque on an ellipsoid in a flow field having deformation and angular velocity (vorticity). To express the torque components, it is necessary to calculate the flow velocity gradients in the body-fixed frame,

$$\nabla \mathbf{V_b} = \mathbf{Q} \cdot (\nabla \mathbf{V_e}) \cdot \mathbf{Q^{-1}} \quad \text{and} \quad \nabla \mathbf{V_e} = \begin{pmatrix} \frac{\partial Vx}{\partial x} & \frac{\partial Vx}{\partial y} & \frac{\partial Vx}{\partial z} \\ \frac{\partial Vy}{\partial x} & \frac{\partial Vy}{\partial y} & \frac{\partial Vy}{\partial z} \\ \frac{\partial Vz}{\partial x} & \frac{\partial Vz}{\partial y} & \frac{\partial Vz}{\partial z} \end{pmatrix} \tag{A.15}$$

where the subscripts b and e relate to the body-fixed frame and the earth-fixed (inertial) frame, respectively.

The deformation rate and vorticity are

$$\gamma_{32} = \frac{1}{2}\left[(\nabla \mathbf{V_b})_{3,2} + (\nabla \mathbf{V_b})_{2,3})\right], \quad \gamma_{13} = \tfrac{1}{2}\left[(\nabla \mathbf{V_b})_{1,3} + (\nabla \mathbf{V_b})_{3,1})\right], \tag{A.16}$$

$$\omega_1 = \frac{1}{2}\left[(\nabla \mathbf{V_b})_{3,2} - (\nabla \mathbf{V_b})_{2,3})\right], \quad \omega_2 = \tfrac{1}{2}\left[(\nabla \mathbf{V_b})_{1,3} - (\nabla \mathbf{V_b})_{3,1})\right], \quad \omega_3 = \frac{1}{2}\left[(\nabla \mathbf{V_b})_{2,1} - (\nabla \mathbf{V_b})_{1,2})\right].$$

Notice that the vorticity in the body-fixed frame is the transformation of the same quantity in the inertial frame, as described in equation 3.5 (Page 11).

The torque components are now given in the body-fixed frame by

$$\begin{aligned} \sum M_X &= \frac{16\pi\mu a^3\beta}{3(\beta_o + \beta^2\gamma_o)}\left[(1-\beta^2)\gamma_{32} + (1+\beta^2)(\omega_1 - p)\right] \\ \sum M_Y &= \frac{16\pi\mu a^3\beta}{3(\beta_o + \beta^2\gamma_o)}\left[(\beta^2-1)\gamma_{13} + (1+\beta^2)(\omega_2 - q)\right] \\ \sum M_Z &= \frac{32\pi\mu a^3\beta}{3(\beta_o + \alpha_o)}(\omega_3 - r) \end{aligned} \tag{A.17}$$

where

$$\alpha_o = \beta_o = \frac{\beta^2}{\beta^2-1} + \frac{\beta}{2(\beta^2-1)^{3/2}} \ln\left(\frac{\beta - \sqrt{\beta^2-1}}{\beta + \sqrt{\beta^2-1}}\right) \tag{A.18}$$

$$\gamma_o = \frac{-2}{\beta^2-1} - \frac{\beta}{2(\beta^2-1)^{3/2}} \ln\left(\frac{\beta - \sqrt{\beta^2-1}}{\beta + \sqrt{\beta^2-1}}\right) \tag{A.19}$$

The trajectory equations for rotation assumed by Zhang et al. (2001) require the ellipsoid center of buoyancy and center of mass to coincide. In terms of the angular velocities, the equations of rotational velocities are

$$\begin{aligned} I_{xx}\dot{p} + (I_{zz} - I_{yy})qr &= \sum M_X \\ I_{yy}\dot{q} + (I_{xx} - I_{zz})pr &= \sum M_Y \\ I_{zz}\dot{r} + (I_{yy} - I_{xx})pq &= \sum M_Z \end{aligned} \tag{A.20}$$

where moments of inertia are given for an ellipsoid as

$$m = \frac{4}{3}\pi a^3 \beta \rho_o, \quad I_{xx} = I_{yy} = \frac{(1+\beta^2)a^2}{5}m, \quad I_{zz} = \frac{2a^2}{5}m \tag{A.21}$$

In the context of the more general situation when center of mass is not located at the center of the ellipsoid. Let $(0, 0, z_g)$ indicate the location of center of mass relative to the ellipsoid center, the rotation would be expressed by the following

$$\begin{aligned} I_{xx}\dot{p} + (I_{zz} - I_{yy})qr - m z_g(\dot{v} - wq + ur) &= \sum M_X - z_g W Q_{2,3} \\ I_{yy}\dot{q} + (I_{xx} - I_{zz})pr + m z_g(\dot{u} - vr + wq) &= \sum M_Y + z_g W Q_{1,3} \\ I_{zz}\dot{r} + (I_{yy} - I_{xx})pq &= \sum M_Z \end{aligned} \tag{A.22}$$

where W is the weight of the particle. Note that moment of inertial need to be re-calculated due to the offset of geometric center and mass center.

The final equations for simulation of an ellipsoidal particle are obtained by substituting equations A.2, A.5, and A.12 into the equations of translational motion, and including the equations of rotational motion (equation A.22 and the properties of quaternion representation (equations 4.5 and 4.7).

Appendix B

Nomenclature

Appendix B: Nomenclature

The following is a list of the symbols and their definitions used in this document. As a common practice, symbols in bold face are defined as vectors or tensors, and symbols dotted above are time derivative in their own coordinate systems.

$\mathbf{A}$	Homogeneous transform matrix given a set of roll, pitch, and yaw angles
$A_{i,j}$	components of transform matrix $\mathbf{A}$, $i, j = 1,2,3$
A_f	Frontal area of Sensor Fish, $\pi(d/2)^2$
A_p	Projected area of Sensor Fish, πdL
B	Magnitude of buoyancy
$\mathbf{C}$	6×6 matrix of coefficient on the left side of 6DOF motion equations
C_D	axial drag coefficient
$\mathbf{F_A}$	Resultant of forces due to added mass in body-fixed frame
$\mathbf{F_D}$	Resultant of drag forces in body-fixed frame
$\mathbf{F_{HS}}$	Resultant of hydrostatic forces in body-fixed frame
$\mathbf{F_L}$	Resultant of lift forces in body-fixed frame
$\mathbf{H}$	Inverse of coefficient matrix C, C^{-1}
$\mathbf{I}$	Inertial tensor of a rigid body
I_{ij}	Components of inertial tensor in body-fixed frame, $i, j = x,y,z$
$\mathbf{I}'$	Normalized inertial tensor of a rigid body, I/m
I'_{ij}	Components of normalized inertial tensor in body-fixed frame, $I'_{ij} = I_{ij}/m, \quad i, j = x,y,z$
$\mathbf{J}$	Transform matrix for rotational velocities given a set of roll, pitch, and yaw angles
K_A	Resultant of moments due to added mass along body-fixed X-axis
$K_{A\dot{p}}$	Coefficients of moments due to added mass in body-fixed frame
K_D	Resultant of drag moments along body-fixed X-axis
K_{Dww}	Drag moment coefficient in body-fixed frame
K_{HS}	Resultant of hydrostatic moments along body-fixed X-axis
K_L	Resultant of lift moments along body-fixed X-axis
L	Length of Sensor Fish
$\mathbf{M_A}$	Resultant of moments due to added mass in body-fixed frame
M_A	Resultant of moments due to added mass along body-fixed Y-axis
M_{Ai}	Coefficients of moments due to added mass in body-fixed frame, $i = \dot{w}, \dot{q}, uw, vp, rp, uq$
$\mathbf{M_D}$	Resultant of drag moments in body-fixed frame
M_D	Resultant of drag moments along body-fixed Y-axis
M_{Dww}	Drag moment coefficient in body-fixed

frame

M_{Dqq} Drag moment coefficient in body-fixed frame

$\mathbf{M_{HS}}$ Resultant of hydrostatic moments in body-fixed frame

M_{HS} Resultant of hydrostatic moments along body-fixed Y-axis

$\mathbf{M_L}$ Resultant of lift moments in body-fixed frame

M_L Resultant of lift moments along body-fixed Y-axis

M_{Luw} Lift moment coefficient along body-fixed Y-axis

N_A Resultant of moments due to added mass along body-fixed Z-axis

N_{Ai} Coefficients of moments due to added mass in body-fixed frame, $i = \dot{v}, \dot{r}, uv, wp, pq, ur$

N_D Resultant of drag moments along body-fixed Z-axis

N_{Dvv} Drag moment coefficient in body-fixed frame

N_{Drr} Drag moment coefficient in body-fixed frame

N_{HS} Resultant of hydrostatic moments along body-fixed Z-axis

N_L Resultant of lift moments along body-fixed Z-axis

N_{Luv} Lift moment coefficient along body-fixed Z-axis

$\mathbf{Q}$ Transformation matrix in terms of quaternion components

$Q_{i,j}$ Components of transform matrix Q, $i, j = 1, 2, 3$

Re Reynolds number based on slip velocity of Sensor Fish, $U_{slip}L/\nu$

T_i Non-acceleration terms defined in Equation 4.2, $i = 1, 2, 3$

U_{slip} Slip velocity of Sensor Fish

V_1 Axial velocity (X-axis) of ambient flow field in body-fixed frame

$\dot{V}_1$ Axial acceleration (X-axis) of ambient flow field in body-fixed frame, $\frac{dV_1}{dt}$

V_2 Spanwise velocity (Y-axis) of ambient flow field in body-fixed frame

$\dot{V}_2$ Spanwise acceleration (Y-axis) of ambient flow field in body-fixed frame, $\frac{dV_2}{dt}$

V_3 Vertical velocity (Z-axis) of ambient flow field in body-fixed frame

$\dot{V}_3$ Vertical acceleration (Z-axis) of ambient flow field in body-fixed frame, $\frac{dV_3}{dt}$

V_x Axial velocity (x-axis) of ambient flow field in inertial frame

$\dot{V}_x$ Axial acceleration (x-axis) of ambient flow field in inertial frame, $\frac{dV_x}{dt}$

V_y Spanwise velocity (y-axis) of ambient flow field in inertial frame

$\dot{V}_y$ Spanwise acceleration (y-axis) of ambient flow field in inertial frame, $\frac{dV_y}{dt}$

V_z Vertical velocity (z-axis) of ambient flow field in inertial frame

$\dot{V}_z$ Vertical acceleration (z-axis) of ambient flow field in inertial frame, $\frac{dV_z}{dt}$

W Weight of Sensor Fish

X_A Resultant of forces due to added mass along body-fixed X-axis

X_{Ai} Coefficients of forces due to added mass in body-fixed frame, $i = \dot{u}, wq, qq, vr, rr$

X_D Resultant of drag forces along body-fixed X-axis

X_{Duu} Drag coefficient in body-fixed frame

X_{HS} Resultant of hydrostatic forces along body-fixed X-axis

X_L Resultant of lift forces along body-fixed X-axis

Y_A Resultant of forces due to added mass along body-fixed Y-axis

Y_{Ai} Coefficients of forces due to added mass in body-fixed frame, $i = \dot{v}, \dot{r}, ur, wp, pq$

Y_D Resultant of drag forces along body-fixed Y-axis

Y_{Dvv} Drag coefficient in body-fixed frame

Y_{Drr} Drag coefficient in body-fixed frame

Y_{HS} Resultant of hydrostatic forces along body-fixed Y-axis

Y_L Resultant of lift forces along body-fixed Y-axis

Y_{Luv} Lift coefficient along body-fixed Y-axis

Z_A Resultant of forces due to added mass along body-fixed Z-axis

Z_{Ai} Coefficients of forces due to added mass in body-fixed frame, $i = \dot{w}, \dot{q}, uq, vp, rp$

Z_D Resultant of drag forces along body-fixed Z-axis

Z_{Dww} Drag coefficient in body-fixed frame

Z_{Dqq} Drag coefficient in body-fixed frame

Z_{HS} Resultant of hydrostatic forces along body-fixed Z-axis

Z_L Resultant of lift forces along body-fixed Z-axis

Z_{Luw} Lift coefficient along body-fixed Y-axis

$c_{yd\beta}$ Hoerner lift slope coefficient

$c_{y\beta}$ An empirical coefficient for evaluation of $c_{yd\beta}$

d Diameter of Sensor Fish

f_i Non-acceleration terms defined in Equation 4.2, $i = 1, 2, 3$

m Mass of Sensor Fish

p Angular velocity of Sensor Fish with respect to body-fixed X-axis

$\dot{p}$ Rate of change of angular velocity with respect to body-fixed X-axis, $\frac{dp}{dt}$

q Angular velocity of Sensor Fish with respect to body-fixed Y-axis

$\dot{q}$ Rate of change of angular velocity with respect to body-fixed Y-axis, $\frac{dq}{dt}$

r Angular velocity of Sensor Fish with respect to body-fixed Z-axis

$\dot{r}$ Rate of change of angular velocity with respect to body-fixed Z-axis, $\frac{dr}{dt}$

t Time

u Axial velocity of Sensor Fish in body-fixed frame

$\dot{u}$ Axial acceleration of Sensor Fish in body-fixed frame, $\frac{du}{dt}$

v Spanwise velocity of Sensor Fish in body-fixed frame

$\dot{v}$ Spanwise acceleration of Sensor Fish in body-fixed frame, $\frac{dv}{dt}$

$\tilde{v}_i$ Redundant notation of six velocity components, $(u,\ v,\ w,\ p,\ q,\ r)^T$

w Vertical velocity of Sensor Fish in body-fixed frame

$\dot{w}$ Vertical acceleration of Sensor Fish in body-fixed frame, $\frac{dw}{dt}$

x	Axial position of Sensor Fish with respect to inertial frame
$\dot{x}$	Axial velocity of Sensor Fish in inertial frame, $\frac{dx}{dt}$
x_b	Axial position of center of buoyancy in body-fixed frame
x_{cp}	Location of resultant lift in body-fixed frame
x_g	Axial position of center of mass in body-fixed frame
y	Spanwise position of Sensor Fish with respect to inertial frame
$\dot{y}$	Spanwise velocity of Sensor Fish in inertial frame, $\frac{dy}{dt}$
y_b	Spanwise position of center of buoyancy in body-fixed frame
y_g	Spanwise position of center of mass in body-fixed frame
z	Vertical position of Sensor Fish with respect to inertial frame
$\dot{z}$	Vertical velocity of Sensor Fish in inertial frame, $\frac{dz}{dt}$
z_b	Vertical position of center of buoyancy in body-fixed frame
z_g	Vertical position of center of mass in body-fixed frame
ε	Quaternion, $(\varepsilon_1, \varepsilon_2, \varepsilon_3, \varepsilon_4)^T$
ε_1	First component of quaternion ε
ε_2	Second component of quaternion ε
ε_3	Third component of quaternion ε
ε_4	Fourth component of quaternion ε
θ	Pitch angle of Sensor Fish with respect to inertial frame
$\dot{\theta}$	Angular velocity of Sensor Fish with respect to inertial y-axis, $\frac{d\theta}{dt}$
ν	Kinematic viscosity of water
ρ	Density of water
ρ_o	Density of Sensor Fish or the underwater rigid-body
ϕ	Roll angle of Sensor Fish with respect to inertial frame
$\dot{\phi}$	Angular velocity of Sensor Fish with respect to inertial x-axis, $\frac{d\phi}{dt}$
ψ	Yaw angle of Sensor Fish with respect to inertial frame
$\dot{\psi}$	Angular velocity of Sensor Fish with respect to inertial z-axis, $\frac{d\psi}{dt}$
Ω	Angular velocity vector of Sensor Fish with respect to body-fixed frame, $(p,\ q,\ r)^T$
ω_1	Angular velocity of ambient flow with respect to body-fixed X-axis
$\dot{\omega}_1$	Rate of change of ambient flow angular velocity with respect to body-fixed X-axis, $\frac{d\omega_1}{dt}$
ω_2	Angular velocity of ambient flow with respect to body-fixed Y-axis
$\dot{\omega}_2$	Rate of change of ambient flow angular velocity with respect to body-fixed Y-axis, $\frac{d\omega_2}{dt}$
ω_3	Angular velocity of ambient flow with respect to body-fixed Z-axis
$\dot{\omega}_3$	Rate of change of ambient flow angular velocity with respect to body-fixed Z-axis, $\frac{d\omega_3}{dt}$
ω_x	Angular velocity of ambient flow with respect to inertial x-axis
$\dot{\omega}_x$	Rate of change of ambient flow angular velocity with respect to inertial x-axis,

$\frac{d\omega_x}{dt}$

ω_y Angular velocity of ambient flow with respect to inertial y-axis

$\dot{\omega}_y$ Rate of change of ambient flow angular velocity with respect to inertial y-axis, $\frac{d\omega_y}{dt}$

ω_z Angular velocity of ambient flow with respect to inertial z-axis

$\dot{\omega}_z$ Rate of change of ambient flow angular velocity with respect to inertial z-axis, $\frac{d\omega_z}{dt}$

$\nabla \mathbf{V_b}$ Gradient tensor of ambient flow velocity in body-fixed frame

$\nabla \mathbf{V_e}$ Gradient tensor of ambient flow velocity in inertial frame

$\sum \mathbf{F}$ Resultant of external forces in body-fixed frame

$\sum F_X$ Resultant of external forces along body-fixed X-axis

$\sum F'_X$ Normalized resultant of external forces along body-fixed X-axis, $\sum F_X / m$

$\sum F_Y$ Resultant of external forces along body-fixed Y-axis

$\sum F'_Y$ Normalized resultant of external forces along body-fixed Y-axis, $\sum F_Y / m$

$\sum F_Z$ Resultant of external forces along body-fixed Z-axis

$\sum F'_Z$ Normalized resultant of external forces along body-fixed Z-axis, $\sum F_Z / m$

$\sum \mathbf{M}$ Resultant of external moments in body-fixed frame

$\sum M_X$ Resultant of external forces with respect to body-fixed X-axis

$\sum M'_X$ Normalized resultant of external moments with respect to body-fixed X-axis, $\sum M_X / m$

$\sum M_Y$ Resultant of external forces with respect to body-fixed Y-axis

$\sum M'_X$ Normalized resultant of external moments with respect to body-fixed Y-axis, $\sum M_Y / m$

$\sum M_Z$ Resultant of external forces with respect to body-fixed Z-axis

$\sum M'_Z$ Normalized resultant of external moments with respect to body-fixed Z-axis, $\sum M_Z / m$